https://doi.org/10.5194/egusphere-2023-1210
Preprint. Discussion started: 6 July 2023

Individual Coal Mine Methane Emissions Constrained by Eddy-Covariance Measurements: Low Bias and Missing Sources

Kai Qin[1#], Wei Hu[1#], Qin He[1], Fan Lu[1], Jason Blake Cohen[1*]

[1]Jiangsu Key Laboratory of Coal-Based Greenhouse Gas Control and Utilization, School of Environment and Spatial Informatics, China University of Mining and Technology, Xuzhou,221116, China

# These authors contributed equally to this work.

Correspondence to: Jason B.Cohen (jasonbc@alum.mit.edu ; jasonbc@cumt.edu.cn)

Abstract. China's Shanxi Province accounts for 12 % of global coal output, and therefore is responsible for a very large fraction of the total global methane (CH_4) emissions, as well as being a large source of uncertainty due to the lack of in-situ and field measurements. This work introduces the first comprehensive attempt to compute the coal mine methane emissions (CMM) throughout Shanxi, using a mixture of bottom-up and top-down approaches. First, public and private data from 636 individual coal mines in Shanxi Province were analyzed following the IPCC Tier 2 approach, using three to five sets of observed emission factors, and rank information based on methods issued by the National Coal Mine Safety Administration and the National Energy Administration, to compile a range of bottom-up CMM on a mine-by-mine basis. An eddy-covariance tower is set up near the output flue of a well-characterized high rank coal mine in Changzhi, and used to produce an average observed CH_4 flux over two two-month long periods (Winter 2021 and Autumn 2022). The observed half-hourly CH_4 flux variability is found to be roughly stable over the entire observed time, and is subsequently used to produce a set of scaling factors (RATIO correction) to updating the preliminary bottom-up coal mine methane emissions to account for both bias and high-frequency temporal variabiliy. The resulting emissions dataset have been compared against commonly used global CMM datasets including EDGAR and GFEI v2, and yield three unique scientific conclusions. First, their total CH4 emissions over Shanxi lie in between this work's 50th percentile and 70th percentile range, meaning they are slightly high. Second, both datasets

https://doi.org/10.5194/egusphere-2023-1210
Preprint. Discussion started: 6 July 2023

have a very large amount of emissions which occur where there are no coal mines and no CH4 emitting industry, indicating that there are significant spatial disparities, with the overlapped portion of CMM emissions where mines exist consistently close to the 30th percentile of this work's emissions, meaning they underestimate CMM in general on a mine-by-mine basis. Third, some of the mines have average emissions values which are more than the 90th percentile of the computed mine-by-mine emissions, while many are far below the 10th percentile, showing that there is a significant issue with the sampling not capturing the observed temporal variability. It is hoped that this mine-by-mine and high frequency approximation of CMM emissions can improve both top-down observation campaigns as well as provide quantitative support and identification of mitigation opportunities.

1 Introduction

Methane (CH_4) is the second most significant long lived greenhouse gases (GHGs) in terms of net global radiative forci ng after carbon dioxide (CO_2), with a radiative forcing of 0.54±0.11 W m^{-2}, about a quarter of the value for CO_2 (Forster, 202 1). Due to its relatively shorter atmospheric lifetime, efforts to control methane emissions will lead to a more rapid reduction in the current increase in global radiative forcing, and help provide more time for solutions that address CO_2 and ultra long li ved GHGs (Nisbet et al., 2020). The major sources that contribute to global CH_4 emissions include fossil fuel extraction (coa l, oil, and gas), leakage (piping, transport, and at the end user's side), rice paddies, swamps, peatlands, rubbish decay, and ani mal husbandry, with anthropogenic sources compromising roughly 50-65 % of the total (Schwietzke et al., 2016).

For these reasons, developing an accurate, precise, and comprehensive inventory of methane emissions is fundamental to addressing climate change (United States Environmental Protection Agency, 2023; The Global Emissions Initiative, 2023; European et al., 2021; Saunois et al., 2020). Coal mining has been determined to be the fourth largest source of anthropogenic methane emissions, with global coal mine methane (CMM) emissions estimates ranging from 29-61 Tg yr^{-1} (Saunois et al.,

https://doi.org/10.5194/egusphere-2023-1210
Preprint. Discussion started: 6 July 2023

2020). According to Hmiel et al. (2020), anthropogenic fossil CH_4 emissions now account for about 30 % of the global CH_4 source and nearly half of anthropogenic emissions. Based on these results, an improved understanding of the emissions of anthropogenic fossil CH_4 emissions, in particular CMM emissions, will prove critical to the overall goal of emission reductions and climate mitigation (Christensen et al., 2019; Perez-Dominguez et al., 2021; Ou et al., 2021).

One of the current approaches for determining emissions is based on bottom-up aggregation, where observations, laboratory experiments, or processes-based models of emissions are made over a finite number of locations, which are the subsequently scaled up to larger spatial and/or temporal scales. These measurements can include specific sources natural wetlands, cropland, anthropogenic sources, and more. The extracted values are sometimes of related substances, not the species directly wanted, in which cases various different scaling factors are applied to link the concentrations or emissions to each other. Such inventories used in global models are typically constructed from estimates of economic, industrial, residential, transport, power, and other anthropogenic activities combined with emissions factors (Bond et al., 2004; European et al., 2021; Crippa et al., 2021; Oreggioni et al., 2021).

Presently, CMM emissions are produced according to procedures agreed upon under the United Nations Framework Convention on Climate Change (UNFCCC). First, national GHG inventories are produced following one or more of three different tier-based approaches (Christian Boettcher (Germany) et al., 2019). The Tier 1 approach requires that countries choose from a global average range of emission factors and use country-specific activity data to calculate total emissions, resulting in high levels of uncertainty and large representation error (a factor of 2 or more). The Tier 2 approach uses country- or basin-specific emission factors that represent the average values over the coal mines considered, resulting in emissions with moderate amounts of error (at least 50-75%), including respresentation errors associated with variance in coal mine size, operations, and CH_4 geology (William Irving, 2000; Hiller et al., 2014; Maasakkers et al., 2016; Peng et al., 2016; Sheng et al., 2017; Hoesly et al., 2018; Mcduffie et al., 2020; Scarpelli et al., 2020; Deng et al., 2022; Sadavarte et al., 2022; Scarpelli

https://doi.org/10.5194/egusphere-2023-1210
Preprint. Discussion started: 6 July 2023

et al., 2022; Singh et al., 2022). Presently, most countries produce coal mine CH_4 inventories following one of these two approaches. The Tier 3 approach requires both local measurements and facility level data, with the results expected to be more representative in terms of spatial location and inventory categories, as well as likely having both higher accuracy and precision. However, due to the size of the resources required, as well as the lack of availability of such facility level data in most cases, few inventories are currently compiled using this approach (Allen et al., 2013; Miller et al., 2013; Chen et al., 2017).

Brandt et al. (2014) reviewed 20 years of literature and found that emissions inventories across all scales consistently underestimate observed CH_4 emissions fluxes. To compensate for these discrepencies, there is some work which has proposed a hybrid approach that falls somewhere between Tiers 2 and 3. This approach specifically adapts mine-specific or basin-specific emission factors based on a small set of observations, and then extends these values over their entire study area (Ju et al., 2016; Wang et al., 2013). However, these works are few and far between and there is no consistent study bounding the uncertainty of these approaches.

Another approach to estimating emissions is the so-called top-down approach, which involves using in-situ atmospheric observations from individual measurements, observation networks, satellites, etc., in connection with atmospheric transport models, climate models, and even simplified box models which attempt to simulate the transport and in-situ chemical and physical processing. These results are inverted or maximially optimized, deriving an inference of the emissions and some range of uncertainty, which depends on both the observations themselves, as well as the model used (Ehhalt, 1974; Blake et al., 1982; Buchwitz et al., 2005; Chen and Prinn, 2006; Krings et al., 2013; Turner et al., 2015; Varon et al., 2020; Kostinek et al., 2021; Sadavarte et al., 2021; Sanchez-Garcia et al., 2022). The approach generally takes one of two different forms: the first where a small number of long term, high frequency surface flux measurements in space are used to invert the emissions based on a combination of atmospheric variability and atmospheric transport (Andrews et al., 2014); and the second where remotely

https://doi.org/10.5194/egusphere-2023-1210
Preprint. Discussion started: 6 July 2023

sensed columns from satellite or aircraft are analyzed and used to compute the change in the observed variability spatially over a singe or set of a few well defined point sources (Duren et al., 2019; Frankenberg et al., 2016).

The second set of approaches may allow individual point sources to be inverted with a high degree of certainty, but also must be analyzed carefully and the results treated with extreme caution (Varon et al., 2020). First, they need to carefully account for clouds, aerosols, and other undesireable co-contaminants which are present in the field of view when the observations are made (Gifford, 1968; Wolfe et al., 2002; Mears and Wentz, 2005; Delwart et al., 2008; Marland, 2008). Second, they require independent validation, which is site specific (Cressot et al., 2014; Wecht et al., 2012). Third, their overpass frequency is generally not as high as surface measurements, and therefore they may not be sufficiently representative of the actual distribution of emissions in space and time (Vaughn et al., 2018).

While there has been a considerable amount of work using observations in situ to approximation the emissions with respect to short lived species including NO_x (Li et al., 2023), CO (Shan et al., 2019; Feng et al., 2020; Lin et al., 2020), and BC (Bond et al., 2004; Cohen and Wang, 2014), such work with respect to CH_4 from coal mines is only much more recent. An overview of results at the global-scale using top-down approaches have constrainted the global fossil fuel emissions of CH_4 fall within the range of 81-131 Tg yr^{-1} (Zhang et al., 2013; Arad et al., 2014; Fiehn et al., 2020; Varon et al., 2020; Hendel et al., 2021; Kostinek et al., 2021; Krautwurst et al., 2021; Sadavarte et al., 2021; Luther et al., 2022; Swolkien et al., 2022). On the regional scale, the estimation of methane emissions is far less precise, in terms of both magnitude and uncertainty range, especially so at higher temporal frequency (Oberschelp et al., 2019). Due to the large magnitude of the uncertainties and the lack of precision at high temporal and spatial resolution, works which calculate observed trends frequently can not even agree on the magnitude of the sign of the trend, with some studies finding an increase in CMM emissions (Jackson et al., 2020; Stavert et al., 2022) and others show a decline in CMM emissions (Gao et al., 2021). Direct comparisons between top-down

https://doi.org/10.5194/egusphere-2023-1210
Preprint. Discussion started: 6 July 2023

and bottom-up emissions datasets are also quite substantial in terms of all of: magnitude, space, time, and emissions type/sector, leading to ongoing active academic debate (Allen, 2016).

This study proposes a new tailored approach which is based on the strengths of both bottom-up and top-down approaches. First, this work develops a bottom-up set of emissions values on a mine-by-mine basis using different technology and uncertainty parameters over coal-rich Shanxi Province. Second, this work uses eddy covariance observations of actual CH_4 fluxes at high temporal resolution over many months from a single site located within a coal mining company near the exit ventilation shaft. This work then develops a RATIO-correction factor between the computed and observed coal mine emissions at this mine, and then applies this set of RATIO-corrections to every individual mine, considering the uncertainty and probability distributions of both the observations and each individual mine's technical emissions distribution. This work specifically focuses on Shanxi province due to two facts: first that it accounts for 12% of global mining output and therefore is a significant source of CMM CH_4, and second that there is relatively open and high quality data available at the mine-by-mine level. This work aims to produce an emissions dataset on a mine-by-mine basis that is inclusive on of the variable geography, surface versus underground mining approahces, and both active and abandoned mine status. A comprehensive dataset of estimates of CMM emissions on a mine-by-mine, type-by-type, and day-by-day basis is derived, including robust uncertainty analysis.

2 Data and methods

An overview of the methods used in this work is provided in Fig. 1. Measurements of activity data and rank (a qualitative measure of the air flow coming out from the mine) on a mine-by-mine basis are gathered. Different sets of emissions are computed using a bottom-up technology- and geology-based approach on a mine-by-mine basis. Simultaneously, 55 days of continuous measurements, taken over two separate periods in 2021 and 2022 using a high frequency eddy covariance flux

https://doi.org/10.5194/egusphere-2023-1210
Preprint. Discussion started: 6 July 2023

tower are made over different seasons of the year at one of the coal mines in the region, which was specifically selected due to its high quality data and being of typical rank. High frequency statistics from the flux observations are used to both scale the uncertainty range and compute the bias of the average annual CMM emissions from the mine. There is an explicit consideration of the uncertainties from both the bottom-up and top-down emissions approaches. These correction factors are then applied to the other 635 mines in Shanxi. Emissions in terms of average conditions, temporal variation, and extreme events are quantified. Comparisons are made with other existing bottom-up approaches in terms of space and time, revealing errors and biases in terms of the locations and magnitudes of known, misidentified, and previously missing sources.

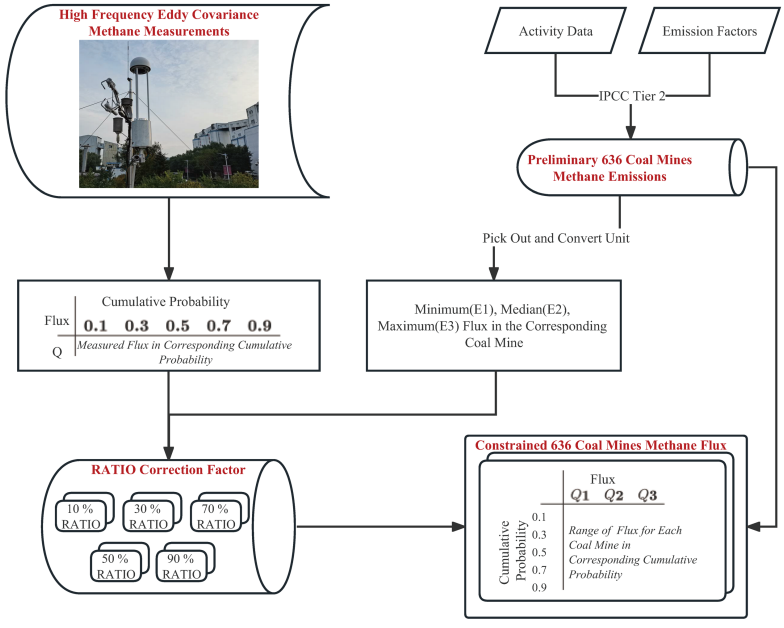

Figure 1: Overview of the methods used in this work.

2.1 Geographic Boundaries of Study Region

Shanxi province in China is one of the major coal producing regions in the world, currently accounting for 12. % of the total global coal output. A map of Shanxi province and 636 individual coal mines identified in this work is displayed in Fig.

https://doi.org/10.5194/egusphere-2023-1210
Preprint. Discussion started: 6 July 2023

2. The overall geospatial distribution includes both open-pit and underground coal mines, as well as those mines which are both actively in use and others which have already been abandoned.

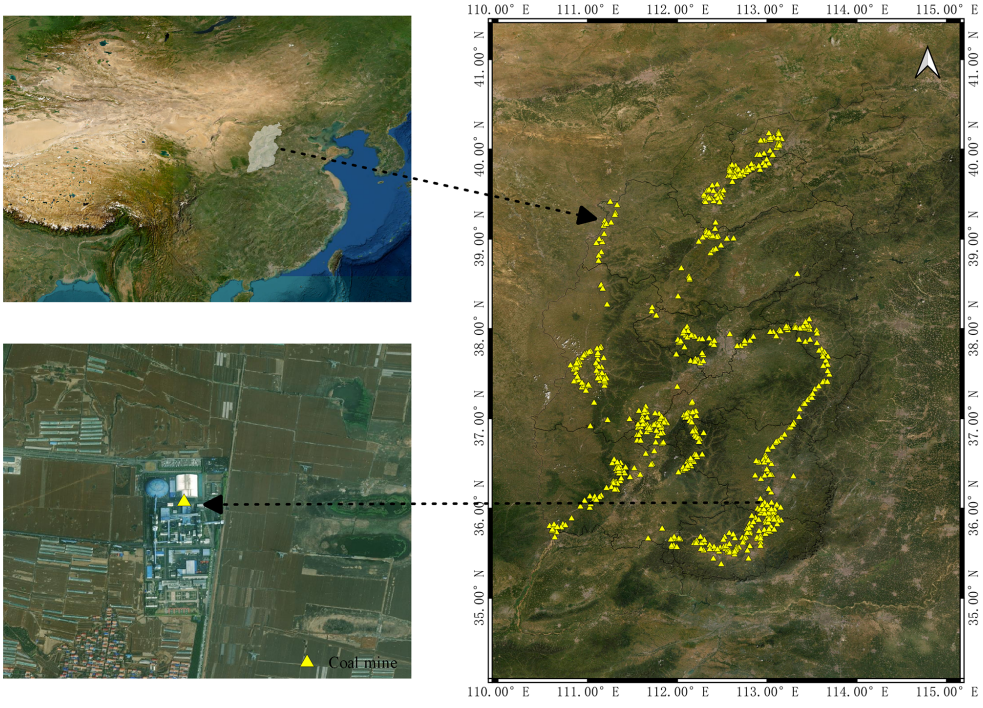

Figure 2: (Top left) location of Shanxi within Asia, (right) map of Shanxi with all individual coal mines given as yellow triangles, and (bottom left) visible image of an individual coal mine (map from ESRI).

2.2 Coal Mine Emissions Data

Each mine and shaft are geolocated using the coal company's name obtained from the Shanxi Provincial Energy Administration and location data from Baidu Map service. To account for the offsets from conversions of different coordinate

https://doi.org/10.5194/egusphere-2023-1210
Preprint. Discussion started: 6 July 2023

systems and potential changes in mine locations or ownership, each location is verified using aerial imagery from ESRI Basemap and Google Earth. The specific geolocation using WGS-84 is presented in Fig. 2.

The bottom-up emissions are computed following the IPCC guidelines for national greenhouse gas inventories Tier 2 methodology, specifically including a factor of human activity (AD), a coefficient that quantifies the amount of emission per unit of activity (EFs), and a conversion factor (CF) to transform the emissions into units of mass of CH_4. Emissions are conceptually computed following Eq. (1), where EFs (m^3 ton^{-1}) is the volume of CH_4 emitted per ton of coal mined and is a function of the activity data used, AD (ton yr^{-1}) is the amount of coal produced by each individual mine, and CF is a conversion factor considering the local atmospheric pressure and ideal gas equation (Christian Boettcher (Germany) et al., 2019).

$$\text{Emissions} = \text{AD} \cdot \text{EFs} \cdot \text{CF} \quad (1)$$

Following the procedures in China, information on the AD is provided on a company-by-company basis while EFs are computed based on the mine rank. All coal mines currently in active use in Shanxi Province post detailed information on both their AD and rank, which is available for download at http://nyj.shanxi.gov.cn/mkscnldxgscysxxgg/ggl, following the approach of (National Mine Safety Administration, 2018). In this work, the values of AD are directly used, while four different ranks are used, consisting of “low gas mine”, “high gas mine”, “gas outburst mine”, and “Default”. Each of these ranks corresponds to a specific range of values of emissions factors as explained in mode detail below. Although individual coal mines are required to report the coal mine rank results, only 406 mines analyzed in this work have reported this data, with the authors setting the remaining 230 coal mines to have a “default” rank.

The emission factors depend strongly on the type of coal extracted (for example, but not limited to: brown coal, hard coal, and sea coal), the way in which it is extracted (underground mining versus surface mining), the geological underground structure (which varies based on region-specific observations) and basin uplift history, and the technologies used to extract the coal, among other factors (Zhou et al., 2021). To better constrain the range of emissions factors, a literature review was

https://doi.org/10.5194/egusphere-2023-1210
Preprint. Discussion started: 6 July 2023

conducted to obtain a range of observed values of EFs as a function of mine rank and type. For surface mines, the EFs were used from Zheng et al. (2005). For underground mines, a set of two to five different values were used, with two papers providing EFs over each of the four ranks (Wang et al., 2013; Gao et al., 2021), and three additional papers providing EFs only over the first three ranks used in this work (Huang et al., 2019; Sheng et al., 2019; Wang et al., 2019), as displayed in Table S1. This work aims to be technology neutral, and therefore all five values of EFs are considered equally likely for each mine over each of the first three categories of rank. At the mines of default rank, since there are only two different EF values given, a third value is calculated based on the weighted EF values of the low rank and high rank mines, with details presented in Table S1. Subsequently all three of these EFs are considered equally likely for each mine in the default rank. The approach used in this work is consistent with previous studies that have been used to derive bottom-up CMM emissions, although there is no previous work that includes as large a number of ranks and different values of EF as employed herein (Huang et al., 2019; Sheng et al., 2019; Wang et al., 2019; Liu et al., 2021).

2.3 Methane Flux Tower Data

Measurements of high frequency CH_4 flux were made at the XiaHuo Village (xhv) coal mine in Zhangzi District, Changzhi city, Shanxi Province, China, using an Eddy Covariance approach (Goulden et al., 1996) with a CSAT-3 anemometer and LI-7700 and Generic Open Path gas analyzers. The LI-7700 was selected due to its success in constraining CH_4 emissions over terrestrial landscapes (Mcdermitt et al., 2010; Alberto et al., 2014; Peltola et al., 2014; Song et al., 2015; Ge et al., 2018). The observations from LI-7700 are based on a single mode tunable near infrared laser capable of operating at ambient temperature. The CH_4 is computed using wavelength modulation spectroscopy (Silver, 1992) across the 1650 nm band, and demodulates the resulting signal at twice the frequency. The demodulated signal is compared with a reference signal shape to determine CH_4 concentration (Xu et al., 2010).

https://doi.org/10.5194/egusphere-2023-1210
Preprint. Discussion started: 6 July 2023

The location of the flux-tower was placed near the airshaft outflow of a mine, that was selected because it is a known source with an emissions that is somewhat representative of other "high" ranked mines in Shanxi, and therefore would both be expected to have a strong signal, while also being a fairly near the middle of the distribution of total coal mines within Shanxi. The WPL-corrected fluxes are used the compute the emissions flux at 10Hz frequency, following Webb et al. (1980) and Mcdermitt et al. (2010). These fluxes are subsequently downscaled to half hourly frequency by averaging over each continuous 30 minute block from 24 October to 21 December 2021 and again from 15 August to 13 September 2022. In total, there are 1544 available half hourly measurements available in 2021 and 667 available half hourly measurements available in 2022.

The absolute value (direction independent) flux, positive only flux, and negative only flux all appear to have similar is probability density functions (PDF), with the only difference being a very minor offset in the positive flux direction. This is consistent with both positive and negative fluxes being actual fluxes associated with the near surface turbulent flow (Bonan, 2015). Given that that there are no other strong sources or sinks of CH_4 within 1500m except for the coal mine itself, both positive fluxes and the absolute value of negative fluxes are retained for this analysis. Therefore, the probability distribution computed using all fluxes on a 30 minute average basis is considered from this point forward.

2.4 RATIO correction

There have been multiple studies which have estimated emissions using both top-down and bottom-up approaches, and cross-validated the results (Zhang et al., 2018; Long et al., 2021; Ma et al., 2021), but there are few that combine these two methods in tandem (Ho et al., 2019). There are also some hybrid modelling approches that combine characteristics identified with top-down and bottom-up models, but which do not actually use either (Jaccard et al., 2004; Ouyang et al., 2023). This work attempts a new way to perform such a hybrid approach: computing bottom-up emissions following those standard approaches, generating a correction factor between the bottom up emissions and a high frequency top-down flux obseration at

https://doi.org/10.5194/egusphere-2023-1210
Preprint. Discussion started: 6 July 2023

a well known and characterized site, and then using this correction factor to apply to all of the other bottom-up emissions datasets to account for both changes in the mean and statistics, as well as account for high frequency variation.

A correction factor is computed based on the ratio of each individual half hourly average computed flux (Q_j) and the average emissions of that mine E_{mj}. A random sampling of the correction factor is used to generate a PDF of the correction on a half-hourly basis, applied to each local mine's E_{mj}. Statistics of this factor allow for analyzing the uncertainty range with respect to temporal variability as well as an objective way to offset and correct any possible bias in both the mean state and its shape as it is distributed over time.

This ratio Q_j/E_{mj} was then used to scale the emissions of each individual mine. In specific, the annual average emissions of all other coal mines E_{mi} were then multipled by $Q_j/E_{mj}*E_{mi}$ point by point, to yield the emissions distribution of each mine i in a probabilistic manner. Since each mine has three to five different possible bottom up emissions inventory values, each of the minimum, maximum, and median cases is scaled. These different initial emissions values, correspondingly E_{1j}, E_{2j}, and E_{3j} are then applied individually for applications in the rest of this work. The new probability distributions of emissions were gathered mine-by-mine and condition-by-condition, and outputted with the corresponding flux values (Q_i) specifically calculated for the probability distribution at steps of 10 % from 0.1-0.9 in Table S2.

2.5 Statistical methods

To obtain the probabilistic distribution of emissions for each coal mine, a 10,000 member bootstrap was applied (Felsenstein, 1985). This entails first smapling randomly along the domain from [0,1], corresponding to the cumulative probability. This value was then applied to the PDF of observed CH_4 emissions and then applied mine-by-mine computing and applying the RATIO correction factor based on the following piecewise procedure. When the random value falls within the range [0.0,0.2], the 10 % RATIO is selected; when the random value falls within the range [0.2,0.4], the 30 % RATIO is

https://doi.org/10.5194/egusphere-2023-1210
Preprint. Discussion started: 6 July 2023

selected; when the random value falls within the range [0.4,0.6], the 50 % RATIO is selected; when the random value falls within the range [0.6,0.8], the 70 % RATIO is selected; and otherwise the 90 % RATIO is selected.

The resulting distributions were then analyzed over groups of mines based on their bottom-up annual emissions amounts as a function of coal mine rank. Confidence intervals for the fluxes at the different percentiles for each individual coal mine and each grouped set of coal mines by rank and their 95 % confidence interval using the bias corrected and accelerated percentile (Bca) method were computed and are given at https://doi.org/10.6084/m9.figshare.23265644.

2.6 Limitations

The data used to generate the bottom-up emissions is from 2019, while the eddy covariance measurements are made in 2021 and 2022. The EFs are constant from year to year, although there may be interannual variations occurring on a mine-by-mine basis, especially given the unique economic conditions which occurred on the ground in China in 2021 and 2022. There are also uncertainties associated with the variability of the geological conditions encountered as mining expands into new parts of the coal field, and individual mine companies introduce differing new technologies. Since the differences between the measured high frequency CH_4 fluxes is very small between 2021 and 2022, and all of the coal mines analyzed herein are found in the same geographic area and with similar geological conditions, it is assumed these changes are relatively small compared to the actual observed temporal variation in the CH_4 flux observations.

The length of the total dataset was designed to be sufficiently representive of high frequency variations, such as the effects of different anthropogenic activities occurring at during different times of day, different days basis, and changes in activities occurring as policies and changes in demand for coal occur. The methods employed here are not sufficiently long to analyze interannual or intraannual variation.

Despite data limitations, the datasets represent an important step forward regarding the spatial and temporal variability of fluxes among individual coal mines. As described herein, many mines are either missing from inventories entirely or found to

https://doi.org/10.5194/egusphere-2023-1210
Preprint. Discussion started: 6 July 2023

be located in the wrong place. Second, the data computed in this week is more frequent than the 3 monthly observations made to follow the current policies, which is therefore likely missing with respect to monthly-to-annual temporal scales of bottom-up emissions processes. This is likely even larger in terms of undersampling induced biases when using various remotely sensed platforms. However, the length of the dataset and the difficulty of placing a flux tower safely very close to a CH_4 methane outshaft may also lead to a lack of sufficiencly broad representation of true emissions, in particular not successfully sampling all of the extremely high emissions events. For all of these reasons, the results found herein are already likely to be slightly less broad, and therefore on average slightly lower than the emissions actually occurring in the real world.

Further limitations stem from the fact that while this work has obtained measurements and locations from 636 different coal mines companies, only 406 of which contain gas emission rank data. Of these 406 mines containing coal ranks, there are 259, 122 and 25 mines are respectively defined respectively as being low rank, high rank and outburst rank. There are also 13 surface mines. According to China Energy Statistical Yearbook, Shanxi Energy Balance Sheet, Shanxi Province produced 920.3 Tg of raw coal in 2019, with a total of 915.8 Tg collected. The missing 4.5 Tg of raw coal production implies that there are still missing mines and/or companies, or there is significant loss occurring during transport, in both ways pointing out to the fact that there are likely locations which have CMM emissions which are not known in terms of their geospatial locaction. A part of this confusion may also stem from the fact that 50 coal mines were shut down in 2019 due to various environmental and safety concerns. On top of this, there is one abandoned coal mine that exists in the data. There is likely to be some CMM associated with these sites, but which may be outside of the ranges applied in this work to properly analyze.

https://doi.org/10.5194/egusphere-2023-1210
Preprint. Discussion started: 6 July 2023

3 Results and discussion

3.1 Initial Bottom-up CMM emissions

Using emission factors in from Gao et al. (2021), Sheng et al. (2019), Huang et al. (2019), Wang et al. (2013), Zheng et al. (2005), and Wang et al. (2019) in combination with the IPCC Tier 2 approach, the bottom-up emissions from each individual coal mine was calculated. The boxplots of the emissions calculated at three different ranks and under 5 different EFs are show in Fig. 3. First, it is observed that the central 50 % of emissions values is not always consistent. Under low rank conditions, the emissions from EF3 is lower than the group consisting of EF1, EF4, and EF5, while EF2 is higher than the other groups. Under high rank conditions the grouping of the central 50 % of emissions is slightly tighter, with the EF3 emissions lower than but not statistically outside the group consisting of EF2, EF4, and EF5, although it is statistically lower than EF1. The central 50 % of emissions from EF1 is higher than EF3, but is not outside the range of the others. Under outburst rank, although EF3 and EF4 are higher than the others, none are statistically located outside of the central 50 % data of the others. The CMM emissions is quite broad across each each rank, with a range from 0.15-36.4 Gg yr^{-1} at low rank, from 2.41-153. Gg yr^{-1} at high rank, and from 6.58-140. Gg yr^{-1} at outburst rank. All statistics are provided in Fig. 3.

https://doi.org/10.5194/egusphere-2023-1210
Preprint. Discussion started: 6 July 2023

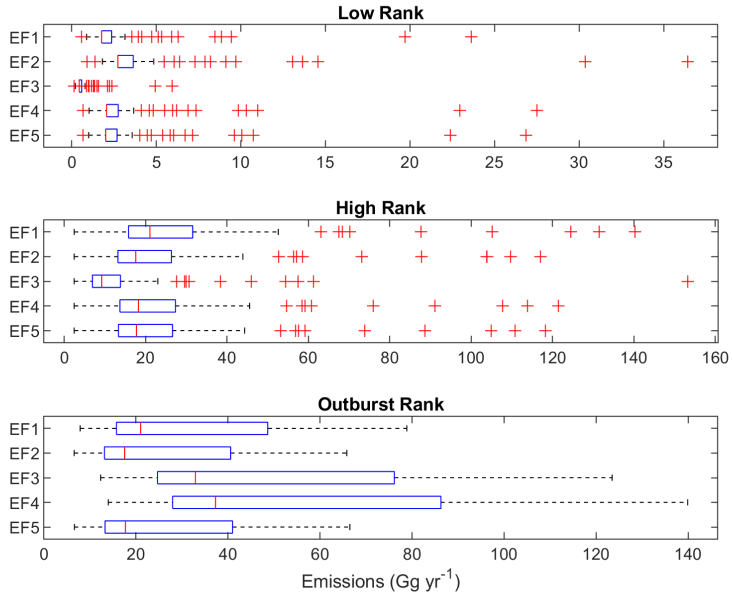

Figure 3: Statistical distribution of bottom-up CH_4 emissions calculated across all mines sorted by: (top) low rank, (middle) high rank, and (bottom) outburst rank. Each box and whisker plot corresponds top to bottom respectively to EFs 1 through EFs 5.

On a Shanxi-wide basis, the range of bottom-up emissions, with the 10th to 90th percentile range of 0.35-1.82 Gg yr^{-1} to 13.8-29.6 Gg yr^{-1}, found to be broader than other works which have estimated CMM, which range from a low of 4.41 Tg yr^{-1} to a high of 7.77 Tg yr^{-1} (Wang et al., 2013; Huang et al., 2019; Sheng et al., 2019; Wang et al., 2019; Gao et al., 2021). The results also are found to be broader than the most widely used bottom-up emission inventories produced using global scale data for CH_4: EDGAR (Oreggioni et al., 2021; Janssens-Maenhout et al., 2019) v6 (Crippa, 2021) and GFEI (Scarpelli et al., 2022; Scarpelli et al., 2020) v2 (Scarpelli and Jacob, 2021), which respectively have 10th and 90th percentile range of 0.77 Gg yr^{-1} to 30.1 Gg yr^{-1} and 0.02 Gg yr^{-1} to 12.9 Gg yr^{-1} in Shanxi.

The reasons why this work's results are broarder than previous works is in part because this work uses multiple independent input databases, while Sheng et al. (2019) and Gao et al. (2021) calculated emissions factors derived from the State Administration of Coal Mine Safety (SACMS), Wang et al. (2019) calculated data from the China High Resolution

https://doi.org/10.5194/egusphere-2023-1210
Preprint. Discussion started: 6 July 2023

Emission Gridded Database (CHRED), and Huang et al. (2019), derived their emission factors from Yuan et al. (2006), which in turn were calculated form the same underlying national level statistics, with data of large key enterprises in China used as supporting data. The reason that EF3 is statistically lower than every other EFs at low rank, and is statistically lower than EF1 at high rank may be in part for two reasons: first that this work does not consider a separate factor for abandoned mines and open-pit mines, while second this work uses a unified gas level statistic for low and high rank mines (Wang et al., 2013). As discussed later in this work, there is further divergence induced by both geospatial and temporal differences between EDGAR and GFEI on one hand, and the high resolution maps with scaled high frequency methane measurements on the other hand, as demonstrated by the maximum and minimum values of EDGAR being (0. and 712.) and GFEI being (0. And 200.) Gg yr^{-1} respectively being far outside of the range of the results herein, even at the highest emitting mine.

3.2 Eddy Covariance Emissions

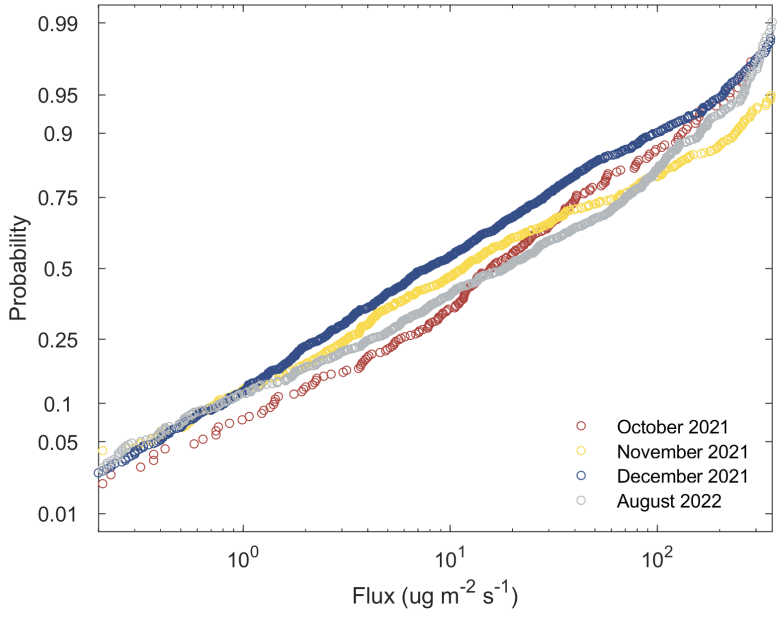

Figure 4: Cumulative probability distribution of 30-minute Eddy Covariance flux measurements ug m^{-2} s^{-1}, where: (red) is October 2021, (yellow) is November 2021, (blue) is December 2021, and (grey) is August 2022. All observations are included in this plot.

https://doi.org/10.5194/egusphere-2023-1210
Preprint. Discussion started: 6 July 2023

The cumulative distribution function (CDF) of 30-minute eddy covariance observations on a month-by-month basis are given in Fig. 4. First, it is observed that the flux in December 2021 is always lower than in the other months, by an average value of 20.4 ug m^{-2} s^{-1}. The other three months have similar mean and median values, with there being only small differences in different probability regions. Specifically in the percentile range around 44.8 %, the flux in August 2022 is at most 2.62 ug m^{-2} s^{-1} lower than in October 2021, and the flux in the percentile range near 68.9 % in November 2021 is at most 5.60 ug m^{-2} s^{-1} lower than in October 2021. Even considering the absolute shift between December 2021 and the other months, the magnitude is relatively small compared with both the median and variance. Therefore, the sampling time is assumed to be sufficient to represent the actual variability in the observed CMM flux over the duration when the observations were made.

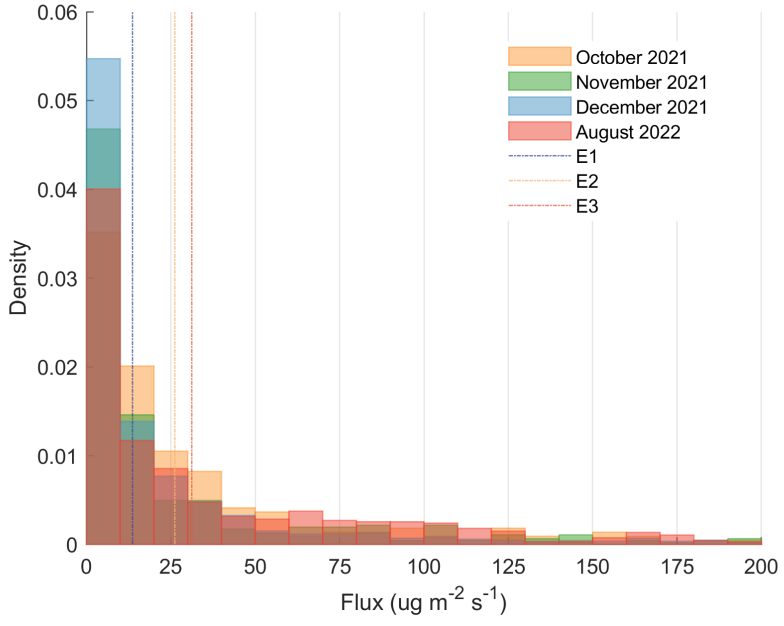

Figure 5: Probability density function of Eddy Covariance fluxes in ug m^{-2} s^{-1} are given as different colored bars over different times: (orange) October 2021, (green) November 2021, (blue) December 2021, and (red) August 2022. Bottom-up emissions fluxes in ug m^{-2} s^{-1} for (E1) minimum flux, (E2) median flux, and (E3) maximum flux, are respectively given as light blue, yellow, and red dash dot vertical lines. Fluxes higher than 200 ug m^{-2} s^{-1} are not shown.

https://doi.org/10.5194/egusphere-2023-1210
Preprint. Discussion started: 6 July 2023

The observed fluxes are presented as a PDF along with the three bottom-up emissions estimations for the same (xhv), presented in Fig. 5. The three vertical lines respectively correspond to the minimum (E_1), median (E_2), and maximum (E_3) bottom-up emission values calculated in Sect. 3.1, which are respectively 13.6, 26.3, and 31.1 ug m^{-2} s^{-1}. While the distribution is clearly skewed, it is not biased, with the boxes covering E_1, E_2, and E_3 representing the central 15.5 % of data, 53.5 % of the data falling into the single box below E_1, and 31.0 % of the data within the remaining boxes above the ceiling of the bottom-up measurements. Similar to (Frankenberg et al., 2016), this work's observations have a long tail and are approximately lognormally distributed.

The bottom-up approach slightly overestimates the median of the emissions distribution (11.7 ug m^{-2} s^{-1}), although it also simultaneously underestimates the mean of the emissions on a mass basis (50.4 ug m^{-2} s^{-1}) due to the the top 14.4 % of emissions being an order of magnitude higher than the median range. The fact means that an insufficiently large sample, such as that which may be made by infrequent overpasses by high resolution satellites or highly intensive but short-duration field campaigns, risk leading to a biased overall respresentation of the emissions. Since the data is sufficiently representative of the overall distribution of bottom-up sources on a daily-scale, the randomly sampled variability of the measurements as a whole are assumed to be a measure of the true variability in time, and this relationship is then applied on a day-to-day basis to scale the annually distributed emissions on a day-by-day basis for further analysis.

The rest of this work outlines the use and impact that scaling the annualized emissions and its uncertainty range on a mine-by-mine basis using the high-frequency variance in time applied in a probabilistic manner. This scaled emissions impacts both the magnitude and variability of E1, E2, and E3 in a way to make them consistent with the statistics and variability of the observations, leading to a new dataset of emissions constructed at all coal mines in Shanxi that shares the same probabilistic variability observed at xhv. This is reasonable given that the high frequency variability is likely linked to the common geology,

https://doi.org/10.5194/egusphere-2023-1210
Preprint. Discussion started: 6 July 2023

economic, and technological conditions found throughout the province, and not due to other external sources, different policies, or differences how the coal is mined and/or processed.

3.3 Constrained CMM Emissions

The RATIO correction factors were applied to every coal mine after conversion of units from Gg yr^{-1} to ug m^{-2} s^{-1}, by assuming the area to be that of the property owned by each coal mining company. In the case where individual mines do not contain sufficient information needed to successfully convert units, this work uses average unit conversion value computed grouping the remaining mines by their rank, with 149 of the total of 636 coal mines falling into this category. For those mines with sufficient information, bootstrap simulation was used to obtain the confidence interval (CI) around the mean. This work then randomly selected data from the central 95 % of the CI corresponding to the rank of the coal mine.

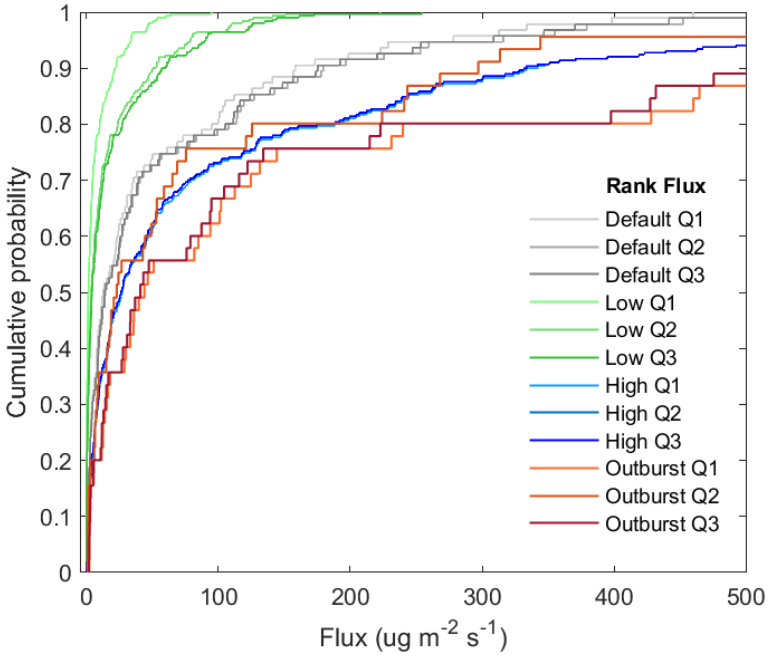

Figure 6: CDFs of emissions as a function of different rank ug m^{-2} s^{-1}. Rank and Q_j (j=1, 2, 3), which are respectively defined and described in Sections 2.2 and Sect. 2.4.

https://doi.org/10.5194/egusphere-2023-1210
Preprint. Discussion started: 6 July 2023

Fig. 6 shows the CDF of emissions fluxes as a function of different ranks and technology levels. Each rank has 3 curves (Q_j, j=1, 2, 3), corresponding to the base cases E_1, E_2, and E_3, with details and statistics of constrained CMM fluxes presented in Table S2. As can be seen across each rank (except for Outburst) that E_1 always has the lowest emissions, E_2 always has intermediate emissions, and E_3 always has the highest relative emissions. With respect to the rank, while low is always lower than default, and default is lower than high or outburst, high and outburst are not always lower or higher than each other. While these findings are generally consistent with the idea that the rank of a coal mine is related to its emisisons, there are exceptions to this general rulk. Since the current treatment of default rank is a linear weighting of low rank and the high rank functions, this itself can be further modified in terms of how many different coal mines there are in each respective weight, allowing the end user of the emissions to rapidly override the assumptions made herein and use the default rank to define any new rank that the user may want.

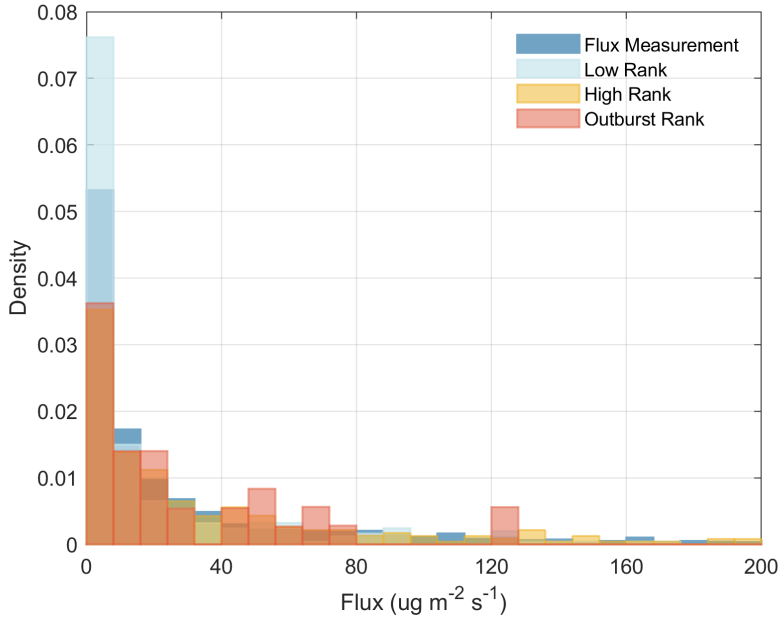

Figure 7: PDF of all calculated emissions fluxes across all mines, separated rank-by-rank in units of ug m^{-2} s^{-1} where: (light blue) is low rank, (yellow) is high rank, and (red) is outburst rank. PDF of flux observations less than 200 ug m^{-2} s^{-1} are given in (dark blue).

https://doi.org/10.5194/egusphere-2023-1210
Preprint. Discussion started: 6 July 2023

PDFs of emissions across all mines on a mine-by-mine basis are analyzed for different ranks in Fig. 7. First, it is clear that the low rank fluxes are lower than the observations. Second, fluxes at both high and outburst ranks generally are found to be larger than the flux observations. However when only considering the set of super high emissions (herein considered to be larger than 100 ug m^{-2} s^{-1}), these conditions consist of 26.5 % of mines with high rank, 22.1 % mines with outburst rank, 14.4 % of the obsewrved fluxes.

3.4 Comparison with existing inventories

The results from this study are compared with multiple existing community emissions databases of CMM that are built using the bottom-up approach including: EDGAR, GFEI, US-EPA Community Emisssions Data System (CEDS) (Mcduffie et al., 2020; Hoesly et al., 2018), and Peking University Emissions database PKU-CH_4 (Liu et al., 2021; Peng et al., 2016). These different datasets estimate their emissions using a consistent approach based on country-specific activity data, emissions factors, and technological abatement when available, and claim to cover all major souce sectors, including fossil fuels, and therefore should be capable of representing CMM emissions. The notable differences include: EDGAR mostly applying a Tier 1 approach, GEFI applying a hybrid Tier 1 and Tier 2 approach depending on data availability, and CEDS scaling pre-existing emissions to match country-specific inventories already reported to the UNFCCC. For these reasons, the different databases can differ from each other in terms of sector-by-sector coverage, geospatial distribution, temporal time averaging, uncertainty range, and how the emissions are mapped, among other differences.

In order to compare with the emissions inventories, all individual mines were summed together on the same spatial grid as EDGAR and GFEI (specifically the emissions of CH_4 from oil, gas, and coal activities in 2019: IPCC Sector 1B1 and 1B2) at 0.1° x 0.1°, allowing analysis on a grid-by-grid basis, with the results shown in Table 1, where cases in which this work's results are both larger than and smaller than EDGAR and GFEI results individually analyzed (included as positive and negative), and differences in the probabilitiy distribution of emissions corrected by the 10 %, 30 %, 50 %, 70 % and 90 %

https://doi.org/10.5194/egusphere-2023-1210
Preprint. Discussion started: 6 July 2023

(included as R1, R3, R5, R7 and R9). Note that all values are computed in terms of Gg d^{-1}, so as to represent the actual variability in the observations made herein, and to understand more deeply how annual and other long-term averages may not be precise without appropriate sampling techniques. While the 90% values look to be quite large, there are many accounts in the real world which match these values, including flux tower observations (Xu et al., 2014), a 20-day study of a well blowout from Ohio which was reported to account for a quarter of the state's annual methane emissions (Pandey et al., 2019), and a large single day's emissions from an undersea gas pipeline explosion (Yu et al., 2022). Therefore, these the 90% values provide an essential quantification of low probability highly emitting events that actually occur in the real world.

Table 1: statistical comparison of emissions in Gg d^{-1}., production in Tg, grid numbers, mine numbers, and rank.

	EDGAR Positive This Work Positive	EDGAR Positive This Work Negative	EDGAR Negative This Work Positive	GFEI Positive This Work Positive	GFEI Positive This Work Negative	GFEI Negative This Work Positive
R1	0.66		0.06	0.72		0.002
R3	3.36		0.33	3.67		0.01
R5	9.49		0.93	10.4		0.03
R7	26.8		2.63	29.3		0.10
R9	122.		11.9	133.		0.43
	14.9	8.04		7.99	11.7	
PRODUCTION(Tg)	839		77.2	909		7.10
GRIDS	201	272	30	227	1114	4
mines			47			5
RANK			22D+16L+7H+2O			2D+3L

Throughout Shanxi, 201 grids have non-zero CMM emissions both from this work and EDGAR, with respective R5 and EDGAR emissions of 9.49 Gg d^{-1} and 14.9 Gg d^{-1}, while 227 grids have non-zero MCC both from this work and GFEI, with respective R5 and GFEI emissions of 10.4 Gg d^{-1} and 7.99 Gg d^{-1}. There are 272 grids where EDGAR has non-zero CMM while this work shows no coal mines, with a total emissions of 8.04 Gg d^{-1}. There are 30 grids where this work has non-zero CMM and EDGAR has no emissions, with a resulting R5 value of 0.93 Gg d^{-1}. These girds contain 47 mines, of which 22 are default rank, 16 are low rank, 7 are high rank and 2 are outburst rank, accounting for a total raw coal production of 77.2 Tg.

https://doi.org/10.5194/egusphere-2023-1210
Preprint. Discussion started: 6 July 2023

There are 1114 grids where GFEI has non-zero CMM while this work shows no coal mines, with a total emissions of 11.7 Gg d^{-1}, between our R5 and R7 values. There are 4 girds where this work has non-zero CMM and GFEI has no emissions, with a resulting R5 value of 0.03 Gg d^{-1}. These 4 grids contain 5 mines, of which 2 are default rank and 3 are low rank, accounting for a total raw coal production of 7.10 Tg.

Mine-by-mine differences between EDGAR and this work's CMM and GFEI and this works CMM are respectively shown in Fig. 8 , where the x-axis represents each individual grid that contains non-zero emissions of both datasets, and the y-axis represents the difference of EDGAR/GFEI – our CMM emissions in units of Gg d^{-1}. EDGAR has 7 grids with values much smaller than R1 (in total summing to 0.014 Gg d^{-1}), 66 grids with values laying between the R3 and R5 values, and a very small number of grids, 12 grids larger than the R9 values. GFEI has 58 grids with values much smaller than R1 (in total summing to 0.13 Gg d^{-1}), 55 grids with values laying between the R3 and R5 values, and a very small number of grids, 10 grids larger than the R9 values. This work's Shanxi-wide results have a bottom-up CMM range of E1 to E3 ranging from 4.41-7.77 Tg yr^{-1}, and a post-correction CMM emissions range at R3, R5, and R7 respectively of [1.35, 3.81, 10.75] Tg yr^{-1}. While both EDGAR and GFEI summed Shanxi-wide are larger than R5 and smaller R7 value, this is not the case when those locations at which there are no mines are removed. EDGAR has a Shanxi-wide CMM of 8.38 Tg yr^{-1}, of which the CMM at locations without mines is 2.94 Tg yr^{-1}. GFEI has a Shanxi-wide CMM of and 7.19 Tg yr^{-1}, of which the CMM at locations without mines is even larger, 4.27 Tg yr^{-1}.

https://doi.org/10.5194/egusphere-2023-1210
Preprint. Discussion started: 6 July 2023

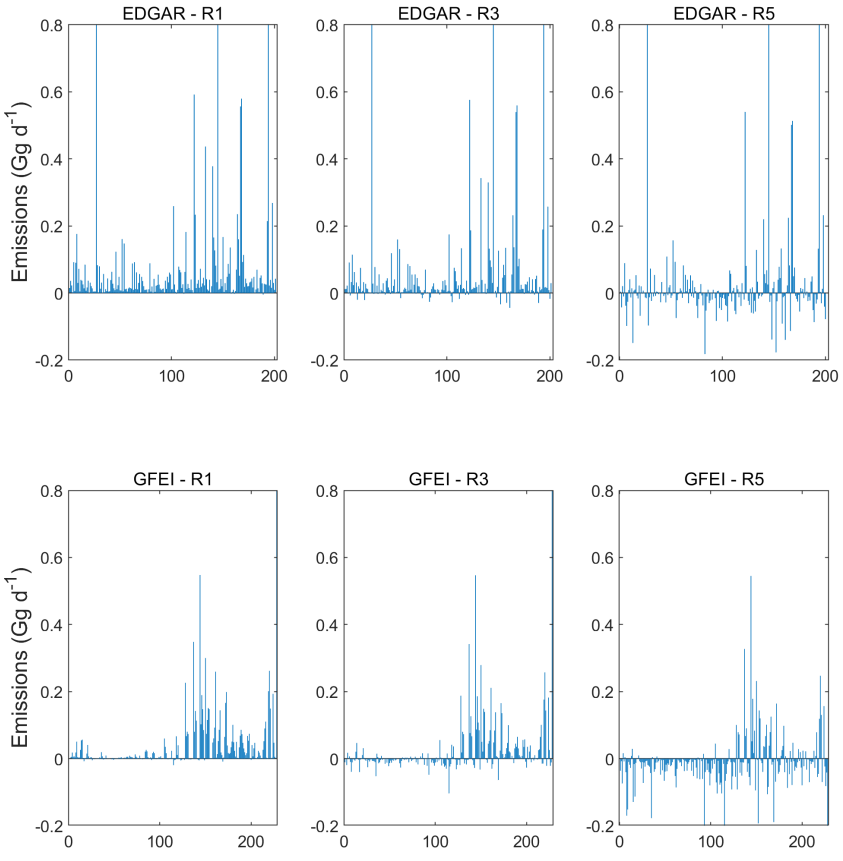

Figure 8: Grid-by-grid difference between EDGAR (top) or GFEI (bottom) and this works respective corrected emissions (left) R1, (center) R3, and (right) R5) with y-axis in units of Gg d^{-1} and x-axis corresponding to each individual grid.

https://doi.org/10.5194/egusphere-2023-1210
Preprint. Discussion started: 6 July 2023

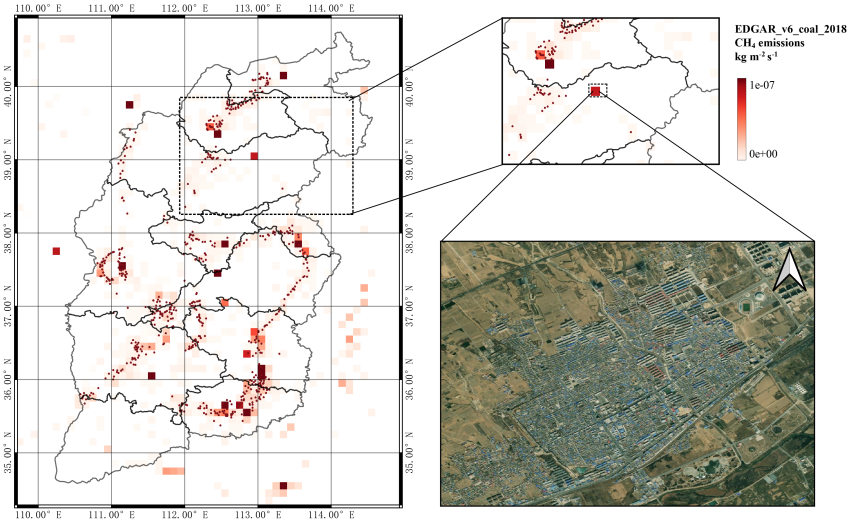

Figure 9: The mapped annual average emissions from EDGAR are overlapped with the locations of the mines used in this work. Note that the region located inside of the black dashed box is shown in more detail on the top right as an EDGAR CH_4 emissions hotspot. However, there are no actual coal mines anywhere in the box. This is supported by the RGB image (from ESRI) of the actual location, which shows a residential area.

To visualize the spatial differences, maps of the grid-by-grid annual average emissions from EDGAR and GFEI are overlapped with the locations of the mines used in this work in Fig. 9 and Fig. 10 respectively. A deeper investigation is made into two sets of regions: those in which this dataset has emissions and there are no emissions in one or both of EDGAR or GFEI, and those regions in which there are no coal mines, but one or both of EDGAR and GFEI have emissions. Both sets of improperly mapped emissions are indicative of systematic bias or error, and can not be corrected merely through scaling (Cohen et al., 2011).

Throughout Shanxi GFEI shows no emissions at 5 mines and extremely low emissions at 5 more mines, while EDGAR shows no emissions at 47 mines and extremely low emissions at 38 additional mines. One specific and fascinating detail to investigate is that the grid in which this works flux tower measurements of CH_4 were made (where xhv is located) happens to

https://doi.org/10.5194/egusphere-2023-1210
Preprint. Discussion started: 6 July 2023

be one of these special grids. EDGAR reports zero emissions and GFEI reports very low emissions, 5.28 ug m^{-2} s^{-1}, while our E1 value is 13.6 ug m^{-2} s^{-1} and our corrected 30% RATIO is 4.13 ug m^{-2} s^{-1}.

For this reason, a comparison on a grid-by-grid and mine-by-mine basis over the entire city of Changzhi is conducted. The Changzhi wide statistics of (minimum, median, maximum, and mean) emission of EDGAR on a grid-by-grid basis where coal mines exist are 0.12, 5.29, 67.7 and 13.2 ug m^{-2} s^{-1}, respectively, while their same statistics within Changzhi on grids which do not have coal emissions are 0.18, 0.55, 36.9, and 4.38 ug m^{-2} s^{-1}. This work's CMM inventory at xhv has values of E1 to E3 ranging from 13.6-31.1 ug m^{-2} s^{-1}, with the corresponding final 10%, 30%, 50%, 70%, and 90% emissions values after RATIO correction being [0.81, 4.13, 11.7, 33.0, 150.] ug m^{-2} s^{-1}, respectively. This indicates that the EDGAR emissions in general have both a lower mean and a narrower distribution as compared with the results within Changzhi, as well as a significant fraction of urban CH_4 emissions mis-identified as being due to fossil fuels..

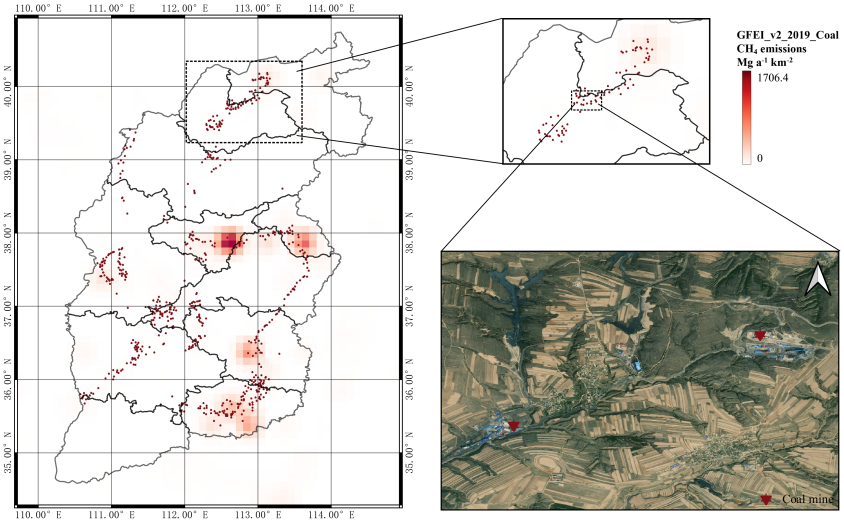

Figure 10: The mapped annual average emissions from GFEI are overlapped with the locations of the mines used in this work. Note that the region located inside of the black dashed box is shown in more detail on the top right as a region with almost zero emissions by GFEI CH_4 emissions. However, there actual location contains multiple coal mines. For ease of viewing, only 2 of the 25 coal mines are shown on the map (from ESRI).

https://doi.org/10.5194/egusphere-2023-1210
Preprint. Discussion started: 6 July 2023

A map of the grid-by-grid average GFEI CMM emissions are overlapped with the locations of the mines used in this work in Fig. 10. As observed, there are some regions which exist in GFEI which also exist in our dataset, there are other regions in GFEI which are not identified in our dataset, and there are regions identified in our dataset which do not exist in GFEI. As demonstrated in Fig. 8, some of the regions containing mines in this work effectively have almost no emissions as reported by GFEI, indicating that there is a spatial mismatch likely. The total emissions in regions which have mines but are not reported by GFEI ranges at E1 from 0.74-10.1 Gg $yr^{-1}$and at E3 from 1.77 to 14.72 Gg yr^{-1}.

In the subregion shown in Fig. 10, GFEI reports emissions at 6 grids, with a range from a minimum of 0.17 Gg yr^{-1} to a maximum of 0.59 Gg yr^{-1}. This work's total emissions over the mines reports emissions at 5 of these grids, while there are none reported at the largest GFEI grid within this region (0.59 Gg yr^{-1}). The emissions calculated by this work's approach at the minimum of these GEFI grids (0.17 Gg yr^{-1}) is computed to have a 30%/50%/70% value of 10.3/29.2/82.3 Gg yr^{-1}, while the emissions at the maximum of these GEFI grids (0.58 Gg yr^{-1}) is calculated to have a 30%/50%/70% value of 12.4/35.2/99.3 Gg yr^{-1}. These findings show that scaling GFEI will not lead to a good match with the CMM emissions, since the magnitudes of the observed mine-by-mine emissions does not order in the same way as the GFEI emissions, and even using different scaling factors for different rank mines would also be insufficient.

There are regions identified in this work at which GFEI and EDGAR both have very high emissions, in which there is actually a large urban center (eastern Taiyuan) or industrial center (southwestern Linfen and northeastern Xinzhou), all without any mines. Another work (Li et al., 2023) identifies industrial boilers as the major source of emissions in one of these regions, some of which are powered by natural gas. Whether such spatial mismatch or mis-identification has occurred, or a more fundamental error in how the CH_4 emissions are partitioned fror industrial sources is unfortunately not provided by the EDGAR or GFEI teams and can not be investigated further.

https://doi.org/10.5194/egusphere-2023-1210
Preprint. Discussion started: 6 July 2023

Following the results of Brandt et al. (2014), measurements at all scales show official inventories underestimate actual CH_4 emissions conservatively defined as 1.25-1.75 times EPA GHGI estimates. For this reason, the R7 value obtained in this work, which is about 1.3-2.4 times higher than bottom-up estimates in coal mining sector, seems to be a decent fit. This concept of official inventories underestimating CMM is further highlighted by the issue of emissions from closed coal mines. Even though the number of coal mines being stopped due to various regulations is increasing, it seems that the quantification of abandoned mine methane (AMM) emissions is not considered reasonably. In this work a single abandoned mine is identified and its R3/R5/R7 emissiosn are calculated to be 0.48/1.35/3.81 Gg yr^{-1}, whichi s much larger than the China-wide AMM emissions of 4.7±0.94 Tg in 2020 produced by Chen et al. (2022).

While there are many such papers making claims that top-down estimates of CH_4 emissions are slightly lower than bottom-up approaches at global scale (i.e. Saunois et al., 2020), there is no actual data available over Shanxi province, and therefore, such a comparison is not possible at the present time. However, Maasakkers et al. (2022) used TROPOMI data to invert CH_4 emissions at a city-level spatial scale and found that the emissions are 1.4 to 2.6 times larger than reported in commonly used emission inventories. While this compares reasonably on average with our mine-by-mine values over the range from R5 to R7, as already detailed above, a more precise grid-by-grid approach is required to make a thorough comparison, since otherwise mis-attribution may play a significant role.

4 Conclusions

This work has compiled a mine-by-mine and high temporal resolution inventory of Shanxi province's 2019 CMM emissions. This inventory provides a specific location for each coal mine, including inactive mines. The technology-based approach first employed produces a range of emissions from 4.41-7.77 Tg CH_4 in 2019. The follow-up approach of scaling the observations based on the PDF analysis of high frequency eddy covariance methane measurements was proposed as a

https://doi.org/10.5194/egusphere-2023-1210
Preprint. Discussion started: 6 July 2023

correction. This set of ratio correction factors was applied and yielded a set of emissions at the 10%,30%,50%,70%, and 90% level of [0.72, 3.69, 10.4, 29.4, 133.] $GgCH_4$ per day. By preparing a PDF, such extreme events as occasionally observed can also be analyzed, consistent with the eddy covariance observations which show a lognormal distribution.

Comparsion between our Bottom-up inventories with EDGAR and GFEI reveal that a proper spatial and temporal comparison is essential. While on a province wide basis both EDGAR and GFEI lies between this work's 50% and 70% values, with EDGAR closer to our 70% value than GFEI, this is not a spatially coherent comparison. While looking only at the geospatial grids which actually contain coal mines, both EDGAR and GFEI are found in our 30% to 50% range, and therefore both underestimate the median emissions. Furthermore, in both cases, on a mine-by-mine basis, the values are generally found to be slightly too low, while there are also some mines which are an order of magnitude or more too high. On top of this, both datasets have a considerable amount of CMM observed in regions which are urban, or which are commercial, and which do not have any mines. This indicates that in general the slightly too low values of EDGAR and GFEI CMM Shanxi-wide is due to a few serious distortions. Specifically, these datasets generally has a low bias and underestimates CMM on the vast majority of grids in which there is overlap. The datasets then offset this bias by a combination in two ways: first through a systematic overestimation of CMM on some grids at the high end of the distribution, and second through including emissions on a large number of grids which do not actually have any coal mines. For this reason, It is essential to analyze the total emissions not only on an overall basis, but also in terms of location, magnitude, and variability, otherwise comparisons with and validation using remotely sensed products and models becomes a case of comparing things that may have the same name, but are actually quite different.

The scaling done in this work is based on 55 days of observations at a single large coal mine. While the results seem relatively consistent month-to-month, the variability may be found to also exhibit a different characteristic if additional sites were analyzed. Furthermore, analyzing different types of sites based not only on production, but also based on different

https://doi.org/10.5194/egusphere-2023-1210
Preprint. Discussion started: 6 July 2023

underlying geological conditions or methods by which the coal was extracted may also provide deeper insights. Given that the wind patterns are different in this region during different phases of both El Niño and La Niña, as well as other dynamical regimes (Baldwin et al., 2001), therefore continuing to measure data over a longer period of time may lead to a further refinement of the probability distribution of the observed fluxes. On top of this, mining leakage or procedures may be different in very cold months from very hot months, and therefore a better representation of the emissions under different temperature conditions, especially with respect to how they change the different mining prodecures may also help to improve the accuracy. The goal is to provide enough data and cover enough cases, as to offer the most improved possible set of observations, so that the more broad and well-supported range of emissions can be constrained, allowing for ultimate development of CMM mitigation.

Comparisons with existing CMM emissions are shown to demonstrate greater spatial and temporal variability, national and international inventories and carbon accounting, and more process and model refinement and development. Although aggregated emissions are genrally of the same order of magnitude at the Province level, there are quantitative differences observed in terms of spatial heterogeneity, source type, and temporal variability between our results and the different inventories. While EDGAR and GFEI have total CMM emissions which are similar, that is in part because both add in extra emissions over regions that do not have mines, and have been indentified in this work clearly as being urban and/or commercial/industrial. In addition to this, both datasets underestimate existing CMM methane on average across most of the mines, but occasionally have a single mine which has an emissions even larger than even the 90% value calculated in this work. As a result, without a precise spatial and temporal distribution, comparisons between top-down estimates from satellite and other attempts at validation of emissions can not be done in a reasonable or consistent manner. This work therefore provides a platform by which a spatially, and temporally quantifiable set of CMM emissions can be obtained. It is hoped that this work can inform or support present and future technical, climate policy, and/or mitigation efforts to understand and control CMM.

https://doi.org/10.5194/egusphere-2023-1210
Preprint. Discussion started: 6 July 2023

Data availability

The EDGAR v6.0 Greenhouse Gas Emissions are available at http://data.europa.eu/89h/97a67d67-c62e-4826-b873-9d972c4f670b. The GFEI v2 are avalibale at https://doi.org/10.7910/DVN/HH4EUM. The individual CMM emissions in Shanxi Province compiled in this study are avialble at https://doi.org/10.6084/m9.figshare.23265644.

Author contributions

Wei Hu, Kai Qin, and Jason Blake Cohen developed the research question and analytical approaches. Hu Wei and Fan Lu performed the field experiments. Qin He gathered the data and Wei Hu performed the data analysis with input from Kai Qin and Jason Blake Cohen. Wei Hu, Kai Qin wrote the first draft of the manuscript while Jason Blake Cohen edited and finalized the manuscript. All authors discussed the results and contributed to the final manuscript.

Competing interests

The authors declare that they have no conflict of interest.

Acknowledgments

We sincerely appreciate all the scientists, engineers, and students who participated in the field campaigns maintained the measurement instruments and collected and processed the data. The study was supported by the Shanxi Province Major Science and Technique Program (202101090301013), National Natural Science Foundation of China (42075147 and 41975041), and the Fundamental Research Funds for the Central Universities (2023KYJD1003).

References

https://doi.org/10.5194/egusphere-2023-1210
Preprint. Discussion started: 6 July 2023

Alberto, M. C. R., Wassmann, R., Buresh, R. J., Quilty, J. R., Correa, T. Q., Sandro, J. M., and Centeno, C. A. R.: Measuring methane flux from irrigated rice fields by eddy covariance method using open-path gas analyzer, Field Crop Res, 160, 12-21, https://doi.org/10.1016/j.fcr.2014.02.008, 2014.

Allen, D.: Attributing Atmospheric Methane to Anthropogenic Emission Sources, Accounts Chem Res, 49, 1344-1350, https://doi.org/10.1021/acs.accounts.6b00081, 2016.

Allen, D. T., Torres, V. M., Thomas, J., Sullivan, D. W., Harrison, M., Hendler, A., Herndon, S. C., Kolb, C. E., Fraser, M. P., Hill, A. D., Lamb, B. K., Miskimins, J., Sawyer, R. F., and Seinfeld, J. H.: Measurements of methane emissions at natural gas production sites in the United States (vol 110, pg 17768, 2013), Proc. Natl. Acad. Sci. U. S. A., 110, 18023-18023, https://doi.org/10.1073/pnas.1304880110, 2013.

Andrews, A. E., Kofler, J. D., Trudeau, M. E., Williams, J. C., Neff, D. H., Masarie, K. A., Chao, D. Y., Kitzis, D. R., Novelli, P. C., Zhao, C. L., Dlugokencky, E. J., Lang, P. M., Crotwell, M. J., Fischer, M. L., Parker, M. J., Lee, J. T., Baumann, D. D., Desai, A. R., Stanier, C. O., De Wekker, S. F. J., Wolfe, D. E., Munger, J. W., and Tans, P. P.: CO2, CO, and CH4 measurements from tall towers in the NOAA Earth System Research Laboratory's Global Greenhouse Gas Reference Network: instrumentation, uncertainty analysis, and recommendations for future high-accuracy greenhouse gas monitoring efforts, Atmos Meas Tech, 7, 647-687, https://doi.org/10.5194/amt-7-647-2014, 2014.

Arad, V., Arad, S., Cosma, V. A., Suvar, M., and Sgem: GAZODINAMIC REGIME ON GEOMECHANICS POINT OF VIEW FOR JIU VALLEY COAL BEDS, 14th International Multidisciplinary Scientific Geoconference (SGEM), Albena, BULGARIA, 17-26, Jun, 2014, 269-276, https://doi.org/10.5593/SGEM2014/B13/S3.036, 2014.

Baidu Map API: https://api.map.baidu.com/lbsapi/getpoint/index.html, last access: 14 March.

https://doi.org/10.5194/egusphere-2023-1210
Preprint. Discussion started: 6 July 2023

Baldwin, M. P., Gray, L. J., Dunkerton, T. J., Hamilton, K., Haynes, P. H., Randel, W. J., Holton, J. R., Alexander, M. J., Hirota, I., Horinouchi, T., Jones, D. B. A., Kinnersley, J. S., Marquardt, C., Sato, K., and Takahashi, M.: The quasi-biennial oscillation, Rev Geophys, 39, 179-229, https://doi.org/10.1029/1999rg000073, 2001.

Blake, D. R., Mayer, E. W., Tyler, S. C., Makide, Y., Montague, D. C., and Rowland, F. S.: Global increase in atmospheric methane concentrations between 1978 and 1980, Geophys Res Lett, 9, 477-480, https://doi.org/10.1029/GL009i004p00477, 1982.

Bonan, G.: Turbulent Fluxes, in: Ecological Climatology, 3 ed., edited by: Bonan, G., Cambridge University Press, Cambridge, 209-217, https://doi.org/10.1017/cbo9781107339200.014, 2015.

Bond, T. C., Streets, D. G., Yarber, K. F., Nelson, S. M., Woo, J. H., and Klimont, Z.: A technology-based global inventory of black and organic carbon emissions from combustion, J Geophys Res-Atmos, 109, https://doi.org/10.1029/2003jd003697, 2004.

Brandt, A. R., Heath, G. A., Kort, E. A., O'Sullivan, F., Petron, G., Jordaan, S. M., Tans, P., Wilcox, J., Gopstein, A. M., Arent, D., Wofsy, S., Brown, N. J., Bradley, R., Stucky, G. D., Eardley, D., and Harriss, R.: Methane Leaks from North American Natural Gas Systems, Science, 343, 733-735, https://doi.org/10.1126/science.1247045, 2014.

Buchwitz, M., de Beek, R., Burrows, J. P., Bovensmann, H., Warneke, T., Notholt, J., Meirink, J. F., Goede, A. P. H., Bergamaschi, P., Körner, S., Heimann, M., and Schulz, A.: Atmospheric methane and carbon dioxide from SCIAMACHY satellite data: initial comparison with chemistry and transport models, Atmos Chem Phys, 5, 941-962, https://doi.org/10.5194/acp-5-941-2005, 2005.

Chen, D., Chen, A., Hu, X., Li, B., Li, X., Guo, L., Feng, R., Yang, Y., and Fang, X.: Substantial methane emissions from abandoned coal mines in China, Environ Res, 214, 113944, https://doi.org/10.1016/j.envres.2022.113944, 2022.

https://doi.org/10.5194/egusphere-2023-1210
Preprint. Discussion started: 6 July 2023

Chen, G. J., Yang, S., Lv, C. F., Zhong, J. A., Wang, Z. D., Zhang, Z. N., Fang, X., Li, S. T., Yang, W., and Xue, L. H.: An improved method for estimating GHG emissions from onshore oil and gas exploration and development in China, Sci Total Environ, 574, 707-715, https://doi.org/10.1016/j.scitotenv.2016.09.051, 2017.

Chen, Y.-H. and Prinn, R. G.: Estimation of atmospheric methane emissions between 1996 and 2001 using a three-dimensional global chemical transport model, J Geophys Res-Atmos, 111, https://doi.org/10.1029/2005jd006058, 2006.

Christensen, T. R., Arora, V. K., Gauss, M., Hoglund-Isaksson, L., and Parmentier, F. W.: Tracing the climate signal: mitigation of anthropogenic methane emissions can outweigh a large Arctic natural emission increase, Scientific Reports, 9, 1146, https://doi.org/10.1038/s41598-018-37719-9, 2019.

Christian Boettcher (Germany), A. G. I., Paul Nzomo Mbuthi (Kenya), Steven J. Oliver (Australia), , Roberta Quadrelli (Italy), C. A. R. U. A., Raquel Rodrigues de Souza (Brazil), , Ajay Kumar Singh (India), M. S. G., Kostyantyn Tadlya (Ukraine), Nina Uvarova (Russia), , John D. Watterson (UK), M. M. W. U., Francis Davison Yamba (Zambia), Shengmin Yu (China), , and (China), a. S. Z.: 2019 Refinement to the 2006 IPCC Guidelines for National Greenhouse Gas Inventories, in, Intergovernmental Panel on Climate Change (IPCC), Switzerland, 2019.

Cohen, J. B. and Wang, C.: Estimating global black carbon emissions using a top-down Kalman Filter approach, J Geophys Res-Atmos, 119, 307-323, https://doi.org/10.1002/2013jd019912, 2014.

Cohen, J. B., Prinn, R. G., and Wang, C.: The impact of detailed urban-scale processing on the composition, distribution, and radiative forcing of anthropogenic aerosols, Geophys Res Lett, 38, https://doi.org/10.1029/2011gl047417, 2011.

Cressot, C., Chevallier, F., Bousquet, P., Crevoisier, C., Dlugokencky, E. J., Fortems-Cheiney, A., Frankenberg, C., Parker, R., Pison, I., Scheepmaker, R. A., Montzka, S. A., Krummel, P. B., Steele, L. P., and Langenfelds, R. L.: On the consistency between global and regional methane emissions inferred from SCIAMACHY, TANSO-FTS, IASI and surface measurements, Atmos Chem Phys, 14, 577-592, https://doi.org/10.5194/acp-14-577-2014, 2014.

https://doi.org/10.5194/egusphere-2023-1210
Preprint. Discussion started: 6 July 2023

Crippa, M., Solazzo, E., Guizzardi, D., Monforti-Ferrario, F., Tubiello, F. N., and Leip, A.: Food systems are responsible for a third of global anthropogenic GHG emissions, Nature Food, 2, 198-209, https://doi.org/10.1038/s43016-021-00225-9, 2021.

Crippa, M. G., Diego; Muntean, Marilena; Schaaf, Edwin; Lo Vullo, Eleonora; Solazzo, Efisio; Monforti-Ferrario, Fabio; Olivier, Jos; Vignati, Elisabetta: EDGAR v6.0 Greenhouse Gas Emissions. European Commission, Joint Research Centre (JRC) [dataset], 2021.

Delwart, S., Bouzinac, C., Wursteisen, P., Berger, M., Drinkwater, M., Martin-Neira, M., and Kerr, Y. H.: SMOS validation and the COSMOS campaigns, Ieee T Geosci Remote, 46, 695-704, https://doi.org/10.1109/TGRS.2007.914811, 2008.

Deng, Z., Ciais, P., Tzompa-Sosa, Z. A., Saunois, M., Qiu, C. J., Tan, C., Sun, T. C., Ke, P. Y., Cui, Y. N., Tanaka, K., Lin, X., Thompson, R. L., Tian, H. Q., Yao, Y. Z., Huang, Y. Y., Lauerwald, R., Jain, A. K., Xu, X. M., Bastos, A., Sitch, S., Palmer, P. I., Lauvaux, T., d'Aspremont, A., Giron, C., Benoit, A., Poulter, B., Chang, J. F., Petrescu, A. M. R., Davis, S. J., Liu, Z., Grassi, G., Albergel, C., Tubiello, F. N., Perugini, L., Peters, W., and Chevallier, F.: Comparing national greenhouse gas budgets reported in UNFCCC inventories against atmospheric inversions, Earth Syst Sci Data, 14, 1639-1675, https://doi.org/10.5194/essd-14-1639-2022, 2022.

Duren, R. M., Thorpe, A. K., Foster, K. T., Rafiq, T., Hopkins, F. M., Yadav, V., Bue, B. D., Thompson, D. R., Conley, S., Colombi, N. K., Frankenberg, C., McCubbin, I. B., Eastwood, M. L., Falk, M., Herner, J. D., Croes, B. E., Green, R. O., and Miller, C. E.: California's methane super-emitters, Nature, 575, 180-184, https://doi.org/10.1038/s41586-019-1720-3, 2019.

Ehhalt, D. H.: The atmospheric cycle of methane, Tellus, 26, 58-70, https://doi.org/10.3402/tellusa.v26i1-2.9737, 1974.

European, C., Joint, R. C. O., J, Guizzardi, D., Schaaf, E., Solazzo, E., Crippa, M., Vignati, E., Banja, M., Muntean, M., Grassi, G., Monforti-Ferrario, F., and Rossi, S.: GHG emissions of all world: 2021 report, Publications Office of the European Union, LU, https://doi.org/10.2760/173513, 2021.

https://doi.org/10.5194/egusphere-2023-1210
Preprint. Discussion started: 6 July 2023

Felsenstein, J.: Confidence Limits on Phylogenies: An Approach Using the Bootstrap, Evolution, 39, 783-791, https://doi.org/10.1111/j.1558-5646.1985.tb00420.x, 1985.

Feng, S., Jiang, F., Wu, Z., Wang, H., Ju, W., and Wang, H.: CO Emissions Inferred From Surface CO Observations Over China in December 2013 and 2017, J Geophys Res-Atmos, 125, https://doi.org/10.1029/2019JD031808, 2020.

Fiehn, A., Kostinek, J., Eckl, M., Klausner, T., Galkowski, M., Chen, J., Gerbig, C., Rockmann, T., Maazallahi, H., Schmidt, M., Korben, P., Necki, J., Jagoda, P., Wildmann, N., Mallaun, C., Bun, R., Nickl, A.-L., Jockel, P., Fix, A., and Roiger, A.: Estimating CH4, CO2 and CO emissions from coal mining and industrial activities in the Upper Silesian Coal Basin using an aircraft-based mass balance approach, Atmos Chem Phys, 20, 12675-12695, https://doi.org/10.5194/acp-20-12675-2020, 2020.

Forster, P., T. Storelvmo, K. Armour, W. Collins, J.-L. Dufresne, D. Frame, D.J. Lunt, T. Mauritsen, M.D. Palmer, M. Watanabe, M. Wild, and H. Zhang: The Earth's Energy Budget, Climate Feedbacks, and Climate Sensitivity, in: In Climate Change 2021: The Physical Science Basis, edited by: Masson-Delmotte, V., P. Zhai, A. Pirani, S.L. Connors, C. Péan, S. Berger, N. Caud, Y. Chen, L. Goldfarb, M.I. Gomis, M. Huang, K. Leitzell, E. Lonnoy, J.B.R. Matthews, T.K. Maycock, T. Waterfield, O. Yelekçi, R. Yu, and B. Zhou, Cambridge University Press, Cambridge, United Kingdom and New York, NY, USA, 923–1054, doi:10.1017/9781009157896.009, 2021.

Frankenberg, C., Thorpe, A. K., Thompson, D. R., Hulley, G., Kort, E. A., Vance, N., Borchardt, J., Krings, T., Gerilowski, K., Sweeney, C., Conley, S., Bue, B. D., Aubrey, A. D., Hook, S., and Green, R. O.: Airborne methane remote measurements reveal heavy-tail flux distribution in Four Corners region, Proc. Natl. Acad. Sci. U. S. A., 113, 9734-9739, https://doi.org/10.1073/pnas.1605617113, 2016.

Gao, J., Guan, C., Zhang, B., and Li, K.: Decreasing methane emissions from China's coal mining with rebounded coal production, Environ Res Lett, 16, 124037, https://doi.org/10.1088/1748-9326/ac38d8, 2021.

https://doi.org/10.5194/egusphere-2023-1210
Preprint. Discussion started: 6 July 2023

Ge, H.-X., Zhang, H.-S., Zhang, H., Cai, X.-H., Song, Y., and Kang, L.: The characteristics of methane flux from an irrigated rice farm in East China measured using the eddy covariance method, Agr Forest Meteorol, 249, 228-238, https://doi.org/10.1016/j.agrformet.2017.11.010, 2018.

Gifford, F. A.: An Outline of Theories of Diffusion in the Lower Layers of the Atmosphere, in: Meteorology and Atomic Energy, 66-116, https://www.osti.gov/servlets/purl/4501607, 1968.

Goulden, M. L., Munger, J. W., Fan, S., Daube, B. C., and Wofsy, S. C.: Measurements of carbon sequestration by long-term eddy covariance: methods and a critical evaluation of accuracy, Global Change Biol, 2, 169-182, https://doi.org/10.1111/j.1365-2486.1996.tb00070.x, 1996.

Hendel, J., Lukanko, L., Macuda, J., Kosakowski, P., and Loboziak, K.: Surface geochemical survey in the vicinity of decommissioned coal mine shafts, Sci Total Environ, 779, 146385, https://doi.org/10.1016/j.scitotenv.2021.146385, 2021.

Hiller, R. V., Bretscher, D., DelSontro, T., Diem, T., Eugster, W., Henneberger, R., Hobi, S., Hodson, E., Imer, D., Kreuzer, M., Künzle, T., Merbold, L., Niklaus, P. A., Rihm, B., Schellenberger, A., Schroth, M. H., Schubert, C. J., Siegrist, H., Stieger, J., Buchmann, N., and Brunner, D.: Anthropogenic and natural methane fluxes in Switzerland synthesized within a spatially explicit inventory, Biogeosciences, 11, 1941-1959, https://doi.org/10.5194/bg-11-1941-2014, 2014.

Hmiel, B., Petrenko, V. V., Dyonisius, M. N., Buizert, C., Smith, A. M., Place, P. F., Harth, C., Beaudette, R., Hua, Q., Yang, B., Vimont, I., Michel, S. E., Severinghaus, J. P., Etheridge, D., Bromley, T., Schmitt, J., Fain, X., Weiss, R. F., and Dlugokencky, E.: Preindustrial (CH4)-C-14 indicates greater anthropogenic fossil CH4 emissions, Nature, 578, 409-+, https://doi.org/10.1038/s41586-020-1991-8, 2020.

Ho, Q. B., Vu, H. N. K., Nguyen, T. T., Nguyen, T. T. H., and Nguyen, T. T. T.: A combination of bottom-up and top-down approaches for calculating of air emission for developing countries: a case of Ho Chi Minh City, Vietnam, Air Qual Atmos Hlth, 12, 1059-1072, https://doi.org/10.1007/s11869-019-00722-8, 2019.

https://doi.org/10.5194/egusphere-2023-1210
Preprint. Discussion started: 6 July 2023

Hoesly, R. M., Smith, S. J., Feng, L., Klimont, Z., Janssens-Maenhout, G., Pitkanen, T., Seibert, J. J., Vu, L., Andres, R. J., Bolt, R. M., Bond, T. C., Dawidowski, L., Kholod, N., Kurokawa, J.-i., Li, M., Liu, L., Lu, Z., Moura, M. C. P., O'Rourke, P. R., and Zhang, Q.: Historical (1750–2014) anthropogenic emissions of reactive gases and aerosols from the Community Emissions Data System (CEDS), Geosci Model Dev, 11, 369-408, https://doi.org/10.5194/gmd-11-369-2018, 2018.

Höglund-Isaksson, L.: Global anthropogenic methane emissions 2005–2030: technical mitigation potentials and costs, Atmos Chem Phys, 12, 9079-9096, https://doi.org/10.5194/acp-12-9079-2012, 2012.

Huang, M., Wang, T., Zhao, X., Xie, X., and Wang, D.: Estimation of atmospheric methane emissions and its spatial distribution in China during 2015, Huanjing Kexue Xuebao/Acta Scientiae Circumstantiae, 39, 1371-1380, 2019.

Jaccard, M., Murphy, R., and Rivers, N.: Energy-environment policy modeling of endogenous technological change with personal vehicles: combining top-down and bottom-up methods, Ecol Econ, 51, 31-46, https://doi.org/10.1016/j.ecolecon.2004.06.002, 2004.

Jackson, R. B., Saunois, M., Bousquet, P., Canadell, J. G., Poulter, B., Stavert, A. R., Bergamaschi, P., Niwa, Y., Segers, A., and Tsuruta, A.: Increasing anthropogenic methane emissions arise equally from agricultural and fossil fuel sources, Environ Res Lett, 15, 071002, https://doi.org/10.1088/1748-9326/ab9ed2, 2020.

Janssens-Maenhout, G., Crippa, M., Guizzardi, D., Muntean, M., Schaaf, E., Dentener, F., Bergamaschi, P., Pagliari, V., Olivier, J. G. J., Peters, J. A. H. W., van Aardenne, J. A., Monni, S., Doering, U., Petrescu, A. M. R., Solazzo, E., and Oreggioni, G. D.: EDGAR v4.3.2 Global Atlas of the three major greenhouse gas emissions for the period 1970–2012, Earth Syst Sci Data, 11, 959-1002, https://doi.org/10.5194/essd-11-959-2019, 2019.

Ju, Y., Sun, Y., Sa, Z., Pan, J., Wang, J., Hou, Q., Li, Q., Yan, Z., and Liu, J.: A new approach to estimate fugitive methane emissions from coal mining in China, Sci Total Environ, 543, 514-523, https://doi.org/10.1016/j.scitotenv.2015.11.024, 2016.

https://doi.org/10.5194/egusphere-2023-1210
Preprint. Discussion started: 6 July 2023

Kostinek, J., Roiger, A., Eckl, M., Fiehn, A., Luther, A., Wildmann, N., Klausner, T., Fix, A., Knote, C., Stohl, A., and Butz, A.: Estimating Upper Silesian coal mine methane emissions from airborne in situ observations and dispersion modeling, Atmos Chem Phys, 21, 8791-8807, https://doi.org/10.5194/acp-21-8791-2021, 2021.

Krautwurst, S., Gerilowski, K., Borchardt, J., Wildmann, N., Galkowski, M., Swolkien, J., Marshall, J., Fiehn, A., Roiger, A., Ruhtz, T., Gerbig, C., Necki, J., Burrows, J. P., Fix, A., and Bovensmann, H.: Quantification of CH4 coal mining emissions in Upper Silesia by passive airborne remote sensing observations with the Methane Airborne MAPper (MAMAP) instrument during the CO2 and Methane (CoMet) campaign, Atmos Chem Phys, 21, 17345-17371, https://doi.org/10.5194/acp-21-17345-2021, 2021.

Krings, T., Gerilowski, K., Buchwitz, M., Hartmann, J., Sachs, T., Erzinger, J., Burrows, J. P., and Bovensmann, H.: Quantification of methane emission rates from coal mine ventilation shafts using airborne remote sensing data, Atmos Meas Tech, 6, 151-166, https://doi.org/10.5194/amt-6-151-2013, 2013.

Li, X., Cohen, J. B., Qin, K., Geng, H., Wu, L., Wu, X., Yang, C., Zhang, R., and Zhang, L.: Remotely Sensed and Surface Measurement Derived Mass-Conserving Inversion of Daily High-Resolution NOx Emissions and Inferred Combustion Technologies in Energy Rich Northern China, EGUsphere [preprint], 2023, 1-30, https://doi.org/10.5194/egusphere-2023-2, 2023.

Lin, C. Y., Cohen, J. B., Wang, S., Lan, R. Y., and Deng, W. Z.: A new perspective on the spatial, temporal, and vertical distribution of biomass burning: quantifying a significant increase in CO emissions, Environ Res Lett, 15, https://doi.org/10.1088/1748-9326/abaa7a, 2020.

Liu, G., Peng, S., Lin, X., Ciais, P., Li, X., Xi, Y., Lu, Z., Chang, J., Saunois, M., Wu, Y., Patra, P., Chandra, N., Zeng, H., and Piao, S.: Recent Slowdown of Anthropogenic Methane Emissions in China Driven by Stabilized Coal Production, Environ Sci Tech Let, 8, 739-746, https://doi.org/10.1021/acs.estlett.1c00463, 2021.

https://doi.org/10.5194/egusphere-2023-1210
Preprint. Discussion started: 6 July 2023

Long, Z., Zhang, Z. L., Liang, S., Chen, X. P., Ding, B. W. P., Wang, B., Chen, Y. B., Sun, Y. Q., Li, S. K., and Yang, T.: Spatially explicit carbon emissions at the county scale, Resour Conserv Recy, 173, https://doi.org/10.1016/j.resconrec.2021.105706, 2021.

Luther, A., Kostinek, J., Kleinschek, R., Defratyka, S., Stanisavljevi, M., Forstmaier, A., Dandocsi, A., Scheidweiler, L., Dubravica, D., Wildmann, N., Hase, F., Frey, M. M., Chen, J., Dietrich, F., Necki, J., Swolkien, J., Knote, C., Vardag, S. N., Roiger, A., and Butz, A.: Observational constraints on methane emissions from Polish coal mines using a ground-based remote sensing network, Atmos Chem Phys, 22, 5859-5876, https://doi.org/10.5194/acp-22-5859-2022, 2022.

Ma, S., Worden, J. R., Bloom, A. A., Zhang, Y. Z., Poulter, B., Cusworth, D. H., Yin, Y., Pandey, S., Maasakkers, J. D., Lu, X., Shen, L., Sheng, J. X., Frankenberg, C., Miller, C. E., and Jacob, D. J.: Satellite Constraints on the Latitudinal Distribution and Temperature Sensitivity of Wetland Methane Emissions, Agu Adv, 2, https://doi.org/10.1029/2021AV000408, 2021.

Maasakkers, J. D., Jacob, D. J., Sulprizio, M. P., Turner, A. J., Weitz, M., Wirth, T., Hight, C., DeFigueiredo, M., Desai, M., Schmeltz, R., Hockstad, L., Bloom, A. A., Bowman, K. W., Jeong, S., and Fischer, M. L.: Gridded National Inventory of U.S. Methane Emissions, Environ Sci Technol, 50, 13123-13133, https://doi.org/10.1021/acs.est.6b02878, 2016.

Maasakkers, J. D., Varon, D. J., Elfarsdottir, A., McKeever, J., Jervis, D., Mahapatra, G., Pandey, S., Lorente, A., Borsdorff, T., Foorthuis, L. R., Schuit, B. J., Tol, P., van Kempen, T. A., van Hees, R., and Aben, I.: Using satellites to uncover large methane emissions from landfills, Sci Adv, 8, https://doi.org/10.1126/sciadv.abn9683, 2022.

Marland, G.: Uncertainties in Accounting for CO2From Fossil Fuels, J Ind Ecol, 12, 136-139, https://doi.org/10.1111/j.1530-9290.2008.00014.x, 2008.

McDermitt, D., Burba, G., Xu, L., Anderson, T., Komissarov, A., Riensche, B., Schedlbauer, J., Starr, G., Zona, D., Oechel, W., Oberbauer, S., and Hastings, S.: A new low-power, open-path instrument for measuring methane flux by eddy covariance, Appl Phys B-Lasers O, 102, 391-405, https://doi.org/10.1007/s00340-010-4307-0, 2010.

https://doi.org/10.5194/egusphere-2023-1210
Preprint. Discussion started: 6 July 2023

McDuffie, E. E., Smith, S. J., O'Rourke, P., Tibrewal, K., Venkataraman, C., Marais, E. A., Zheng, B., Crippa, M., Brauer, M., and Martin, R. V.: A global anthropogenic emission inventory of atmospheric pollutants from sector- and fuel-specific sources (1970–2017): an application of the Community Emissions Data System (CEDS), Earth Syst Sci Data, 12, 3413-3442, https://doi.org/10.5194/essd-12-3413-2020, 2020.

Mears, C. A. and Wentz, F. J.: The effect of diurnal correction on satellite-derived lower tropospheric temperature, Science, 309, 1548-1551, https://doi.org/10.1126/science.1114772, 2005.

Miller, S. M., Wofsy, S. C., Michalak, A. M., Kort, E. A., Andrews, A. E., Biraud, S. C., Dlugokencky, E. J., Eluszkiewicz, J., Fischer, M. L., Janssens-Maenhout, G., Miller, B. R., Miller, J. B., Montzka, S. A., Nehrkorn, T., and Sweeney, C.: Anthropogenic emissions of methane in the United States, Proc. Natl. Acad. Sci. U. S. A., 110, 20018-20022, https://doi.org/10.1073/pnas.1314392110, 2013.

National Mine Safety Administration, N. E. A.: Specification for Identification of Classification of Gassy Mines1004-3438, 78-84, 2018.

Nisbet, E. G., Fisher, R. E., Lowry, D., France, J. L., Allen, G., Bakkaloglu, S., Broderick, T. J., Cain, M., Coleman, M., Fernandez, J., Forster, G., Griffiths, P. T., Iverach, C. P., Kelly, B. F. J., Manning, M. R., Nisbet-Jones, P. B. R., Pyle, J. A., Townsend-Small, A., al-Shalaan, A., Warwick, N., and Zazzeri, G.: Methane Mitigation: Methods to Reduce Emissions, on the Path to the Paris Agreement, Rev Geophys, 58, https://doi.org/10.1029/2019RG000675, 2020.

Oberschelp, C., Pfister, S., Raptis, C., and Hellweg, S.: Global emission hotspots of coal power generation, Nature Sustainability, 2, 113-121, https://doi.org/10.1038/s41893-019-0221-6, 2019.

Ohara, T., Akimoto, H., Kurokawa, J., Horii, N., Yamaji, K., Yan, X., and Hayasaka, T.: An Asian emission inventory of anthropogenic emission sources for the period 1980–2020, Atmos Chem Phys, 7, 4419-4444, https://doi.org/10.5194/acp-7-4419-2007, 2007.

https://doi.org/10.5194/egusphere-2023-1210
Preprint. Discussion started: 6 July 2023

Oreggioni, G. D., Monforti Ferraio, F., Crippa, M., Muntean, M., Schaaf, E., Guizzardi, D., Solazzo, E., Duerr, M., Perry, M., and Vignati, E.: Climate change in a changing world: Socio-economic and technological transitions, regulatory frameworks and trends on global greenhouse gas emissions from EDGAR v.5.0, Global Environ Chang, 70, 102350, https://doi.org/10.1016/j.gloenvcha.2021.102350, 2021.

Ou, Y., Roney, C., Alsalam, J., Calvin, K., Creason, J., Edmonds, J., Fawcett, A. A., Kyle, P., Narayan, K., O'Rourke, P., Patel, P., Ragnauth, S., Smith, S. J., and McJeon, H.: Deep mitigation of CO(2) and non-CO(2) greenhouse gases toward 1.5 degrees C and 2 degrees C futures, Nature Communications, 12, 6245, https://doi.org/10.1038/s41467-021-26509-z, 2021.

Ouyang, Z. T., Jackson, R. B., McNicol, G., Fluet-Chouinard, E., Runkle, B. R. K., Papale, D., Knox, S. H., Cooley, S., Delwiche, K. B., Feron, S., Irvin, J. A., Malhotra, A., Muddasir, M., Sabbatini, S., Alberto, M. C. R., Cescatti, A., Chen, C. L., Dong, J. W., Fong, B. N., Guo, H. Q., Hao, L., Iwata, H., Jia, Q. Y., Ju, W. M., Kang, M., Li, H., Kim, J., Reba, M. L., Nayak, A. K., Roberti, D. R., Ryu, Y., Swain, C. K., Tsuang, B., Xiao, X. M., Yuan, W. P., Zhang, G. L., and Zhang, Y. G.: Paddy rice methane emissions across Monsoon Asia, Remote Sens Environ, 284, https://doi.org/10.1016/j.rse.2022.113335, 2023.

Pandey, S., Gautam, R., Houweling, S., van der Gon, H. D., Sadavarte, P., Borsdorff, T., Hasekamp, O., Landgraf, J., Tol, P., van Kempen, T., Hoogeveen, R., van Hees, R., Hamburg, S. P., Maasakkers, J. D., and Aben, I.: Satellite observations reveal extreme methane leakage from a natural gas well blowout, Proc. Natl. Acad. Sci. U. S. A., 116, 26376-26381, https://doi.org/10.1073/pnas.1908712116, 2019.

Peltola, O., Hensen, A., Helfter, C., Belelli Marchesini, L., Bosveld, F. C., van den Bulk, W. C. M., Elbers, J. A., Haapanala, S., Holst, J., Laurila, T., Lindroth, A., Nemitz, E., Röckmann, T., Vermeulen, A. T., and Mammarella, I.: Evaluating the performance of commonly used gas analysers for methane eddy covariance flux measurements: the InGOS inter-comparison field experiment, Biogeosciences, 11, 3163-3186, https://doi.org/10.5194/bg-11-3163-2014, 2014.

https://doi.org/10.5194/egusphere-2023-1210
Preprint. Discussion started: 6 July 2023

Peng, S., Piao, S., Bousquet, P., Ciais, P., Li, B., Lin, X., Tao, S., Wang, Z., Zhang, Y., and Zhou, F.: Inventory of anthropogenic methane emissions in mainland China from 1980 to 2010, Atmos Chem Phys, 16, 14545-14562, https://doi.org/10.5194/acp-16-14545-2016, 2016.

Perez-Dominguez, I., Del Prado, A., Mittenzwei, K., Hristov, J., Frank, S., Tabeau, A., Witzke, P., Havlik, P., van Meijl, H., Lynch, J., Stehfest, E., Pardo, G., Barreiro-Hurle, J., Koopman, J. F. L., and Sanz-Sanchez, M. J.: Short- and long-term warming effects of methane may affect the cost-effectiveness of mitigation policies and benefits of low-meat diets, Nature Food, 2, 970-980, https://doi.org/10.1038/s43016-021-00385-8, 2021.

Sadavarte, P., Pandey, S., Maasakkers, J. D., van der Gon, H. D., Houweling, S., and Aben, I.: A high-resolution gridded inventory of coal mine methane emissions for India and Australia, Elementa-Sci Anthrop, 10, 1, https://doi.org/10.1525/elementa.2021.00056, 2022.

Sadavarte, P., Pandey, S., Maasakkers, J. D., Lorente, A., Borsdorff, T., van der Gon, H. D., Houweling, S., and Aben, I.: Methane Emissions from Superemitting Coal Mines in Australia Quantified Using TROPOMI Satellite Observations, Environ Sci Technol, 55, 16573-16580, https://doi.org/10.1021/acs.est.1c03976, 2021.

Sanchez-Garcia, E., Gorrono, J., Irakulis-Loitxate, I., Varon, D. J., and Guanter, L.: Mapping methane plumes at very high spatial resolution with the WorldView-3 satellite, Atmos Meas Tech, 15, 1657-1674, 10.5194/amt-15-1657-2022, 2022.

Saunois, M., Stavert, A. R., Poulter, B., Bousquet, P., Canadell, J. G., Jackson, R. B., Raymond, P. A., Dlugokencky, E. J., Houweling, S., Patra, P. K., Ciais, P., Arora, V. K., Bastviken, D., Bergamaschi, P., Blake, D. R., Brailsford, G., Bruhwiler, L., Carlson, K. M., Carrol, M., Castaldi, S., Chandra, N., Crevoisier, C., Crill, P. M., Covey, K., Curry, C. L., Etiope, G., Frankenberg, C., Gedney, N., Hegglin, M. I., Höglund-Isaksson, L., Hugelius, G., Ishizawa, M., Ito, A., Janssens-Maenhout, G., Jensen, K. M., Joos, F., Kleinen, T., Krummel, P. B., Langenfelds, R. L., Laruelle, G. G., Liu, L., Machida, T., Maksyutov, S., McDonald, K. C., McNorton, J., Miller, P. A., Melton, J. R., Morino, I., Müller, J., Murguia-Flores, F., Naik, V., Niwa, Y.,

https://doi.org/10.5194/egusphere-2023-1210
Preprint. Discussion started: 6 July 2023

Noce, S., O'Doherty, S., Parker, R. J., Peng, C., Peng, S., Peters, G. P., Prigent, C., Prinn, R., Ramonet, M., Regnier, P., Riley, W. J., Rosentreter, J. A., Segers, A., Simpson, I. J., Shi, H., Smith, S. J., Steele, L. P., Thornton, B. F., Tian, H., Tohjima, Y., Tubiello, F. N., Tsuruta, A., Viovy, N., Voulgarakis, A., Weber, T. S., van Weele, M., van der Werf, G. R., Weiss, R. F., Worthy, D., Wunch, D., Yin, Y., Yoshida, Y., Zhang, W., Zhang, Z., Zhao, Y., Zheng, B., Zhu, Q., Zhu, Q., and Zhuang, Q.: The Global Methane Budget 2000–2017, Earth Syst Sci Data, 12, 1561-1623, https://doi.org/10.5194/essd-12-1561-2020, 2020.

Scarpelli, T. R. and Jacob, D. J.: Global Fuel Exploitation Inventory (GFEI) (V2), Harvard Dataverse [dataset], https://doi.org/10.7910/DVN/HH4EUM, 2021.

Scarpelli, T. R., Jacob, D. J., Maasakkers, J. D., Sulprizio, M. P., Sheng, J.-X., Rose, K., Romeo, L., Worden, J. R., and Janssens-Maenhout, G.: A global gridded (0.1° × 0.1°) inventory of methane emissions from oil, gas, and coal exploitation based on national reports to the United Nations Framework Convention on Climate Change, Earth Syst Sci Data, 12, 563-575, https://doi.org/10.5194/essd-12-563-2020, 2020.

Scarpelli, T. R., Jacob, D. J., Grossman, S., Lu, X., Qu, Z., Sulprizio, M. P., Zhang, Y., Reuland, F., Gordon, D., and Worden, J. R.: Updated Global Fuel Exploitation Inventory (GFEI) for methane emissions from the oil, gas, and coal sectors: evaluation with inversions of atmospheric methane observations, Atmos Chem Phys, 22, 3235-3249, https://doi.org/10.5194/acp-22-3235-2022, 2022.

Schwietzke, S., Sherwood, O. A., Bruhwiler, L. M. P., Miller, J. B., Etiope, G., Dlugokencky, E. J., Michel, S. E., Arling, V. A., Vaughn, B. H., White, J. W. C., and Tans, P. P.: Upward revision of global fossil fuel methane emissions based on isotope database, Nature, 538, 88-91, https://doi.org/10.1038/nature19797, 2016.

https://doi.org/10.5194/egusphere-2023-1210
Preprint. Discussion started: 6 July 2023

Shan, C., Wang, W., Liu, C., Sun, Y., Hu, Q., Xu, X., Tian, Y., Zhang, H., Morino, I., Griffit, D. W. T., and Velazco, V. A.: Regional CO emission estimated from ground-based remote sensing at Hefei site, China, Atmos Res, 222, 25-35, https://doi.org/10.1016/j.atmosres.2019.02.005, 2019.

Sheng, J.-X., Jacob, D. J., Maasakkers, J. D., Sulprizio, M. P., Zavala-Araiza, D., and Hamburg, S. P.: A high-resolution (0.1° × 0.1°) inventory of methane emissions from Canadian and Mexican oil and gas systems, Atmospheric Environment, 158, 211-215, https://doi.org/10.1016/j.atmosenv.2017.02.036, 2017.

Sheng, J., Song, S., Zhang, Y., Prinn, R. G., and Janssens-Maenhout, G.: Bottom-Up Estimates of Coal Mine Methane Emissions in China: A Gridded Inventory, Emission Factors, and Trends, Environ Sci Tech Let, 6, 473-478, https://doi.org/10.1021/acs.estlett.9b00294, 2019.

Silver, J. A.: Frequency-modulation spectroscopy for trace species detection: theory and comparison among experimental methods, Appl Optics, 31, 707-717, https://doi.org/10.1364/AO.31.000707, 1992.

Singh, A. K., Singh, U., Panigrahi, D. C., and Singh, J.: Updated greenhouse gas inventory estimates for Indian underground coal mining based on the 2019 IPCC refinements, iScience, 25, 104946, https://doi.org/10.1016/j.isci.2022.104946, 2022.

Song, W., Wang, H., Wang, G., Chen, L., Jin, Z., Zhuang, Q., and He, J. S.: Methane emissions from an alpine wetland on the Tibetan Plateau: Neglected but vital contribution of the nongrowing season, J Geophys Res-Biogeo, 120, 1475-1490, https://doi.org/10.1002/2015jg003043, 2015.

Stavert, A. R., Saunois, M., Canadell, J. G., Poulter, B., Jackson, R. B., Regnier, P., Lauerwald, R., Raymond, P. A., Allen, G. H., Patra, P. K., Bergamaschi, P., Bousquet, P., Chandra, N., Ciais, P., Gustafson, A., Ishizawa, M., Ito, A., Kleinen, T., Maksyutov, S., McNorton, J., Melton, J. R., Muller, J., Niwa, Y., Peng, S., Riley, W. J., Segers, A., Tian, H., Tsuruta, A., Yin, Y., Zhang, Z., Zheng, B., and Zhuang, Q.: Regional trends and drivers of the global methane budget, Global Change Biol, 28, 182-200, https://doi.org/10.1111/gcb.15901, 2022.

https://doi.org/10.5194/egusphere-2023-1210
Preprint. Discussion started: 6 July 2023

Swolkien, J., Fix, A., and Galkowski, M.: Factors influencing the temporal variability of atmospheric methaneemissions from Upper Silesia coal mines: a case study from the CoMet mission, Atmos Chem Phys, 22, 16031-16052, https://doi.org/10.5194/acp-22-16031-2022, 2022.

GEIA: Global Emissions InitiAtive: http://www.geiacenter.org, last access: 16 February 2023.

Turner, A. J., Jacob, D. J., Wecht, K. J., Maasakkers, J. D., Lundgren, E., Andrews, A. E., Biraud, S. C., Boesch, H., Bowman, K. W., Deutscher, N. M., Dubey, M. K., Griffith, D. W. T., Hase, F., Kuze, A., Notholt, J., Ohyama, H., Parker, R., Payne, V. H., Sussmann, R., Sweeney, C., Velazco, V. A., Warneke, T., Wennberg, P. O., and Wunch, D.: Estimating global and North American methane emissions with high spatial resolution using GOSAT satellite data, Atmos Chem Phys, 15, 7049-7069, https://doi.org/10.5194/acp-15-7049-2015, 2015.

United States Environmental Protection Agency: Inventory of U.S. Greenhouse Gas Emissions and Sinks 1990-2021, EPA, 2023.

Varon, D. J., Jacob, D. J., Jervis, D., and McKeever, J.: Quantifying Time-Averaged Methane Emissions from Individual Coal Mine Vents with GHGSat-D Satellite Observations, Environ Sci Technol, 54, 10246-10253, https://doi.org/10.1021/acs.est.0c01213, 2020.

Vaughn, T. L., Bell, C. S., Pickering, C. K., Schwietzke, S., Heath, G. A., Petron, G., Zimmerle, D. J., Schnell, R. C., and Nummedal, D.: Temporal variability largely explains top-down/bottom-up difference in methane emission estimates from a natural gas production region, Proc. Natl. Acad. Sci. U. S. A., 115, 11712-11717, https://doi.org/10.1073/pnas.1805687115, 2018.

wandergis: coordTransform_py, GitHub [code], 2015.Wang, K., Zhang, J., Cai, B., and Yu, S.: Emission factors of fugitive methane from underground coal mines in China: Estimation and uncertainty, Appl Energ, 250, 273-282, https://doi.org/10.1016/j.apenergy.2019.05.024, 2019.

https://doi.org/10.5194/egusphere-2023-1210
Preprint. Discussion started: 6 July 2023

Wang, N., Zhu, T., Chen, S., and Luo, D. W.: Study on the Interprovincial Emission Factor of Chinese Coal Mine Methane, Appl Mech Mater, 295-298, 3354-3358, https://doi.org/10.4028/www.scientific.net/AMM.295-298.3354, 2013.

Webb, E. K., Pearman, G. I., and Leuning, R.: Correction of flux measurements for density effects due to heat and water vapour transfer, Q J Roy Meteor Soc, 106, 85-100, https://doi.org/10.1002/qj.49710644707, 1980.

Wecht, K. J., Jacob, D. J., Wofsy, S. C., Kort, E. A., Worden, J. R., Kulawik, S. S., Henze, D. K., Kopacz, M., and Payne, V. H.: Validation of TES methane with HIPPO aircraft observations: implications for inverse modeling of methane sources, Atmos Chem Phys, 12, 1823-1832, https://doi.org/10.5194/acp-12-1823-2012, 2012.

William Irving, O. T.: Energy, in: Good Practice Guidance and Uncertainty Management in National Greenhouse Gas Inventories Intergovernmental Panel on Climate Change (IPCC), Switzerland, 129-144, 2000.

Wolfe, R. E., Nishihama, M., Fleig, A. J., Kuyper, J. A., Roy, D. P., Storey, J. C., and Patt, F. S.: Achieving sub-pixel geolocation accuracy in support of MODIS land science, Remote Sens Environ, 83, 31-49, https://doi.org/10.1016/S0034-4257(02)00085-8, 2002.

Xu, L., Burba, G., Schedlbauer, J. L., Zona, D., McDermitt, D. K., Anderson, T., Oberbauer, S. F., Oechel, W. C., Komissarov, A. V., and Riensche, B.: Eddy Covariance Measurements of Methane Flux at Remote Sites with New Low-Power Lightweight Fast Gas Analyzer,

Xu, L. K., Lin, X. M., Amen, J., Welding, K., and McDermitt, D.: Impact of changes in barometric pressure on landfill methane emission, Global Biogeochem Cy, 28, 679-695, https://doi.org/10.1002/2013gb004571, 2014.

Yu, J. V., Hmiel, B., Lyon, D. R., Warren, J., Cusworth, D. H., Duren, R. M., Chen, Y. L., Murphy, E. C., and Brandt, A. R.: Methane Emissions from Natural Gas Gathering Pipelines in the Permian Basin, Environ Sci Tech Let, 9, 969-974, 10.1021/acs.estlett.2c00380, 2022.

https://doi.org/10.5194/egusphere-2023-1210
Preprint. Discussion started: 6 July 2023

Yuan, B., Nie, Z., and Di, X.: Life cycle inventories of fossil fuels in China (I): Energy sources consumption and direct pollutant emissions, Modern Chemical Industry, 26, 59-62+64, https://doi.org/10.16606/j.cnki.issn0253-4320.2006.03.017, 2006.

Zhang, D., Zang, J., Jiang, Y., and Wang, K.: A new borehole arrangement for draining the methane in mining induced fractured zone and the utilization of the drained methane in Yangquan Nanzhuang Coal Mine, 2nd International Symposium on Mine Safety Science and Engineering, Beijing, PEOPLES R CHINA, February 2014, 299-303, https://doi.org/10.1201/b16606-57, 2014.

Zhang, L., Chen, Y. F., Zhao, Y. H., Henze, D. K., Zhu, L. Y., Song, Y., Paulot, F., Liu, X. J., Pan, Y. P., Lin, Y., and Huang, B. X.: Agricultural ammonia emissions in China: reconciling bottom-up and top-down estimates, Atmos Chem Phys, 18, 339-355, https://doi.org/10.5194/acp-18-339-2018, 2018.

Zheng, S., Wang, Y., and Wang, Z.: Methane emissions to atmosphere from coal mine in China, Safety in Coal Mines, 36, 29-33, 2005.

Zhou, Z., Shi, F., Zhang, Y., Yu, Y., and Tang, S.: Influencing Factors of Gas Emission in Coal Mining Face, Singapore, 08 June 2021, 278-284, https://doi.org/10.1007/978-981-15-8411-4_35,